

Structural Plasticity of NFU1 Upon Interaction with Binding Partners: Insights into the Mitochondrial [4Fe-4S] Cluster Pathway

Stefano Da Vela^{1†‡}, Giovanni Saudino^{2†}, Francesca Lucarelli^{2,3}, Lucia Banci^{2,3}, Dmitri I. Svergun^{1‡} and Simone Ciofi-Baffoni^{2,3*}

1 - EMBL Hamburg Site, c/o DESY, Notkestrasse 85, 22607 Hamburg, Germany

2 - Magnetic Resonance Center CERM, University of Florence, Via Luigi Sacconi 6, 50019 Sesto Fiorentino, Florence, Italy

3 - Department of Chemistry, University of Florence, Via della Lastruccia 3, 50019 Sesto Fiorentino, Florence, Italy

Correspondence to Simone Ciofi-Baffoni: ciofi@cerm.unifi.it (S. Ciofi-Baffoni)

<https://doi.org/10.1016/j.jmb.2023.168154>

Edited by M. Guss

Abstract

In humans, the biosynthesis and trafficking of mitochondrial [4Fe-4S]²⁺ clusters is a highly coordinated process that requires a complex protein machinery. In a mitochondrial pathway among various proposed to biosynthesize nascent [4Fe-4S]²⁺ clusters, two [2Fe-2S]²⁺ clusters are converted into a [4Fe-4S]²⁺ cluster on a ISCA1-ISCA2 complex. Along this pathway, this cluster is then mobilized from this complex to mitochondrial apo recipient proteins with the assistance of accessory proteins. NFU1 is the accessory protein that first receives the [4Fe-4S]²⁺ cluster from ISCA1-ISCA2 complex. A structural view of the protein–protein recognition events occurring along the [4Fe-4S]²⁺ cluster trafficking as well as how the globular N-terminal and C-terminal domains of NFU1 act in such process is, however, still elusive. Here, we applied small-angle X-ray scattering coupled with on-line size-exclusion chromatography and paramagnetic NMR to disclose structural snapshots of ISCA1-, ISCA2- and NFU1-containing apo complexes as well as the coordination of [4Fe-4S]²⁺ cluster bound to the ISCA1-NFU1 complex, which is the terminal stable species of the [4Fe-4S]²⁺ cluster transfer pathway involving ISCA1-, ISCA2- and NFU1 proteins. The structural modelling of ISCA1-ISCA2, ISCA1-ISCA2-NFU1 and ISCA1-NFU1 apo complexes, here reported, reveals that the structural plasticity of NFU1 domains is crucial to drive protein partner recognition and modulate [4Fe-4S]²⁺ cluster transfer from the cluster-assembly site in the ISCA1-ISCA2 complex to a cluster-binding site in the ISCA1-NFU1 complex. These structures allowed us to provide a first rationale for the molecular function of the N-domain of NFU1, which can act as a modulator in the [4Fe-4S]²⁺ cluster transfer.

© 2023 The Author(s). Published by Elsevier Ltd. This is an open access article under the CC BY-NC-ND license (<http://creativecommons.org/licenses/by-nc-nd/4.0/>).

Introduction

In humans, the biosynthesis and trafficking of mitochondrial [4Fe-4S]²⁺ clusters is a highly coordinated process and handled by a complex protein machinery.^{1,2} Multiple mitochondrial pathways have been proposed to be operative in the assembly and trafficking of a [4Fe-4S]²⁺ cluster.^{2–7} A relevant aspect that differentiates the proposed

pathways concerns the molecular function of the accessory protein NFU1. Indeed in a proposed pathway, NFU1 works as a downstream acceptor of a [4Fe-4S]²⁺ cluster, assembled upstream on a protein complex, to mediate the cluster insertion into mitochondrial apo recipient proteins.⁸ In another proposed pathway, NFU1 recruits [2Fe-2S] cluster donors to reductively mediate on itself, with the aid of an electron donor, the formation of

a [4Fe-4S]²⁺ cluster, and then NFU1 conveys this cluster to mitochondrial apo recipient proteins.⁹

Here we focused our attention on the mitochondrial pathway in which NFU1 works as the downstream acceptor of an upstream assembled [4Fe-4S]²⁺ cluster (NFU1-cluster acceptor pathway, hereafter). In the first step of this pathway, it has been shown that a [2Fe-2S]²⁺ cluster is primarily *de novo* assembled on a protein scaffold.^{10–13} Then, two [2Fe-2S]²⁺ clusters are reductively coupled to form a [4Fe-4S]²⁺ cluster on a protein complex formed by ISCA1 and ISCA2 proteins, with the assistance of an electron donor.^{14,15} The formed [4Fe-4S]²⁺ cluster is then transferred to mitochondrial apo recipient proteins.² The latter step occurs with the assistance of accessory proteins that specifically and efficiently drive the final steps of the maturation of mitochondrial [4Fe-4S] proteins.^{16–19} While the assembly process of the [4Fe-4S]²⁺ cluster on the ISCA1-ISCA2 complex has been well documented,^{6,7,14,15,20–24} how the cluster is mobilized from the ISCA1-ISCA2 complex to reach the mitochondrial final targets is still elusive. Nevertheless, accessory proteins that assist [4Fe-4S]²⁺ cluster transfer into apo recipient mitochondrial proteins have been identified.^{8,25–27} Among them, NFU1 accessory protein has the broadest spectrum of preferred physiological target proteins, which are complexes I and II of the mitochondrial respiratory chain and LIAS.^{8,9,16} These *in vivo* findings fully agree with our recent *in vitro* data²⁸ showing that NFU1 is the primary target able to receive the [4Fe-4S]²⁺ cluster assembled on the ISCA1-ISCA2 complex, with no requirements of other accessories proteins to mobilize the [4Fe-4S]²⁺ cluster from the ISCA1-ISCA2 complex to NFU1.

Human NFU1 is a protein composed by globular N-terminal and C-terminal domains (N- and C-domains, hereafter) connected by a flexible linker.^{5,29} While the role of the N-domain of NFU1 is still unknown, the C-domain of NFU1 is involved in [4Fe-4S]²⁺ cluster binding via a conserved CXXC motif located in a solvent-exposed loop.^{5,27} Recently, we investigated the mechanism of the NFU1-mediated [4Fe-4S]²⁺ cluster transfer from the human ISCA1-ISCA2 complex, where the cluster is assembled, to LIAS.^{28,30} From these studies, it resulted that protein–protein recognition is the driving force that moves the cluster to its final destination in a specific manner. We have found indeed that the C-domain of apo NFU1 specifically recognises ISCA1 in the [4Fe-4S]²⁺ ISCA1-ISCA2 hetero-complex to form a ternary complex.²⁸ This ISCA1-NFU1 recognition event drives the [4Fe-4S]²⁺ cluster transfer from the site where the [4Fe-4S]²⁺ cluster is assembled on the ISCA1-ISCA2 complex to another cluster-binding site formed by ISCA1 and the C-domain of NFU1, defined cluster-transfer site hereafter. We also showed that the ternary complex is a labile intermediate that can

evolve, through the release of apo ISCA2, to form a heterodimeric ISCA1-NFU1 complex, where the C-domain of NFU1 shares the [4Fe-4S]²⁺ cluster with ISCA1 in the same way as it was found in the ternary complex.²⁸ Finally, we showed that the heterodimeric [4Fe-4S]²⁺ ISCA1-NFU1 complex is able to transfer its [4Fe-4S]²⁺ cargo to LIAS thanks to a preferential recognition of the C-domain of NFU1 for LIAS with respect to that with ISCA1.³⁰ The latter process leads to the breaking of the ISCA1-NFU1 complex to generate apo ISCA1 and a NFU1-LIAS complex with the [4Fe-4S]²⁺ cluster bound to LIAS. In summary, these molecular studies allowed us to propose a model where the C-domain of NFU1 drives first [4Fe-4S]²⁺ cluster delivery from the ISCA1-ISCA2 complex, where the [4Fe-4S]²⁺ cluster is assembled, to the [4Fe-4S]²⁺ ISCA1-NFU1 intermediate complex, which then specifically guides the [4Fe-4S]²⁺ cluster insertion into LIAS. These sequential molecular events are driven by an interaction affinity gradient of the C-domain of NFU1 increasing from ISCA1 to LIAS.

A structural view of the protein–protein recognition events occurring along the mitochondrial NFU1-cluster acceptor pathway towards mitochondrial apo recipient proteins is, however, still missing. This is mainly because the protein–protein complexes involved in this pathway are challenging to be trapped since the involved proteins display substantial intermolecular and intramolecular conformational motions. Here, we provide structural snapshots of ISCA1-, ISCA2- and NFU1-containing apo complexes involved in mitochondrial [4Fe-4S]²⁺ cluster trafficking. We applied small-angle X-ray scattering coupled with on-line size-exclusion chromatography,³¹ which provides low-resolution structural information ideally suitable for integrative structural modelling of these highly dynamic systems, making use of high-resolution models of single domains and complex subunits and NMR-derived structural constraints. The coordination of the [4Fe-4S]²⁺ cluster in the ISCA1-NFU1 complex, which is the holo complex formed by mixing [4Fe-4S]²⁺ ISCA1-ISCA2 and apo NFU1 proteins,²⁸ was also investigated through a combined application of site-directed mutagenesis and paramagnetic NMR.

Results

Structural information on isolated human apo ISCA1 and apo NFU1 by SEC-SAXS

The first step required to structurally characterize the protein–protein interactions driving the [4Fe-4S]²⁺ cluster trafficking in the mitochondrial NFU1-cluster acceptor pathway involves the investigation of the isolated apo ISCA1, apo ISCA2 and apo NFU1 human proteins. SEC-SAXS data allowed us to obtain a structural

picture of these proteins in solution, which is the fundamental prerequisite for modelling ISCA1-, ISCA2- and NFU1-containing apo complexes. As a SAXS-based structural model of isolated human apo ISCA2 was already available as recently reported by us,²² we have here obtained SAXS-based structural modelling only for isolated human apo ISCA1 and apo NFU1.

At variance with the $[2\text{Fe-2S}]^{2+}$ cluster-bound state of human ISCA1 that forms a stable homodimer,²⁸ apo human ISCA1 tends to self-aggregate, and the protein eluted in multiple, only partially resolved peaks (Figure S1). The most prominent peak at the highest elution volume yielded the SAXS curve in Figure 1A(1). The overall parameters obtained from this curve (Table 1) are in good agreement with a molar mass of monomeric ISCA1 expected from its amino acid sequence, with a mild overestimation of the volume. The $P(r)$ function and the dimensionless Kratky plot (Figure S1) indicate a somewhat elongated globular particle. *Ab initio* modelling by repeating ten DAMMIF runs yielded stable solutions (as judged by NSD < 1³²), all fitting the data at goodness-of-fit $\chi^2 \sim 1.1$. The most representative model is shown in Figure 1B (1). Visual comparison of the multiple *ab initio* models (Figure S1) reveals some localized shape variations near the smaller lobe. This observation may point to the presence of extended features with localized flexibility but could also appear due to small amounts of higher oligomers, not fully

resolved by the SEC, which perturb the lowest angle region of the data. To further validate the solution state of ISCA1 as a monomer with disordered, flexible regions, a hybrid modelling was performed by CORAL. The SAXS curve was fitted employing an atomistic model for the rigid core of ISCA1, comprising residues 24–117, and disordered N- and C-termini (see Materials and Methods section for details). The latter were added by CORAL, with chains of 23 and 12 of dummy residues, respectively. Twenty CORAL runs were performed yielding good fits to the data (final χ^2 in range 1.02–1.24 and the best fit is shown in Figure 2A(1)). All CORAL reconstructions featured extended, unstructured N- and C-termini, pointing away from the rigid core (Figure 2B(1)). This is further corroborated by ISCA1 sequence analysis performed IUPred3A,³³ which predicts that the selected N- and C-terminal segments have a high disorder propensity. Additionally, modelling runs were performed to increase the confidence in this model (see Supplementary Data text), and they corroborate that the two termini are highly dynamic and structurally disordered. It is very likely that the high flexibility and the unstructured nature of both N- and C-termini are the cause of the apo ISCA1 self-aggregation observed *in vitro*. These structural properties might determine protein instability for apo ISCA1 at the physiological conditions. We expect, however, that the latter aspect is precluded because proteomic *in vivo* data suggested that ISCA1 in the mitochondrial matrix is

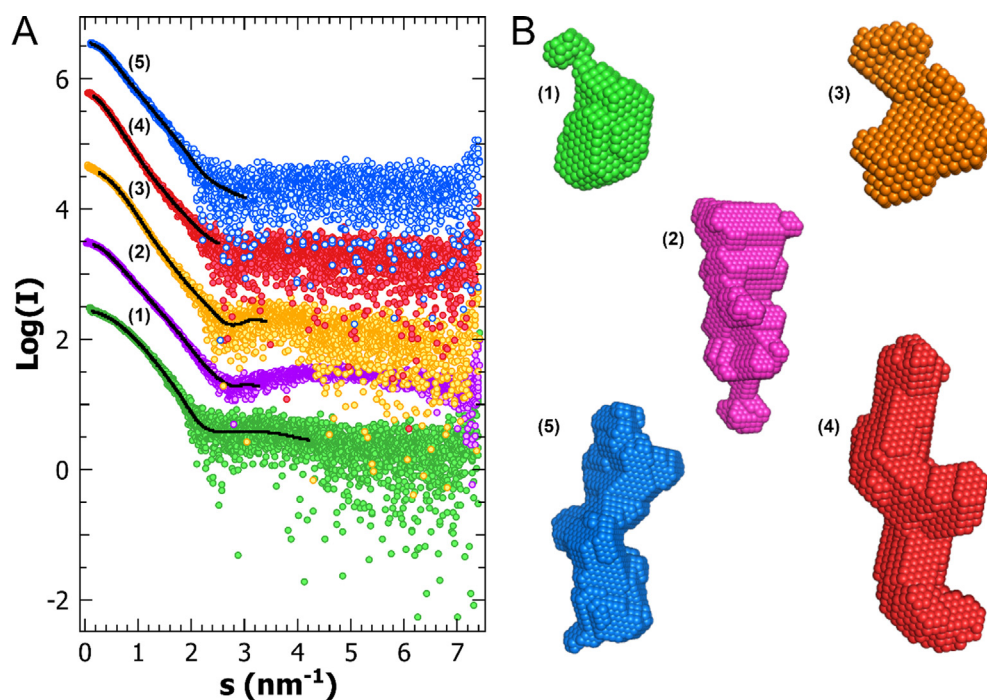


Figure 1. *Ab initio* models of [4Fe-4S] cluster binding proteins and complexes based on SEC-SAXS curves. A. SEC-SAXS curves for (1) apo ISCA1, (2) apo NFU1, (3) apo ISCA1-ISCA2, (4) apo ISCA1-ISCA2-NFU1, (5) apo ISCA1-NFU1, vertically displaced for display. The solid line is the fit of the models in panel B. B. Representative *ab initio* DAMMIF models for the curves in panel A.

Table 1 Overall parameters from the SAXS profiles used for the modelling.

Parameter (unit)	Apo ISCA1	Apo ISCA1-ISCA2	Apo NFU1	Apo NFU1-ISCA1	Apo NFU1-ISCA1-ISCA2
R_g Guinier (nm) ¹	1.90 ± 0.01	2.37 ± 0.01	2.43 ± 0.09	2.64 ± 0.02	3.16 ± 0.06
R_g P(r) (nm) ²	1.94 ± 0.01	2.37 ± 0.01	2.51 ± 0.01	2.73 ± 0.01	3.28 ± 0.01
D_{max} (nm) ³	6.8 ± 0.5	7.8 ± 0.5	9.3 ± 0.5	9.0 ± 0.5	11.7 ± 0.5
Mr Bayes (kDa) ⁴	14.8 (13.8–15.8)	31.6 (29.9–32.8)	23.7 (22.1–25.1)	31.7 (29.9–33.4)	46.7 (45.2–49.2)
V_P (nm ³) ⁵	24.6	42.9	32.1	43.1	69.5
Mr _{VP} (kDa) ⁶	15.4	26.8	20.1	26.9	43.4
Shape class ⁷	compact	compact	extended	extended	flat
Mr _{DATCLASS} ⁸ (kDa)	17.2	31.7	25.4	32.2	53.4
V_{DAM} (nm ³) ⁹	34.6	53.6	41.2	55.3	93.9
Mr _{DAM} (kDa) ¹⁰	17.3	26.8	20.6	27.6	46.9
NSD ¹¹	0.670 ± 0.037	0.763 ± 0.050	0.907 ± 0.031	0.955 ± 0.039	0.858 ± 0.030
Concentration, volume injected (mg/mL, μ L)	7.8, 50	10.6, 40	6.6, 30	10.4, 30	20.4, 30
Mr from sequence (kDa)	14.2	26.7	22.1	36.3	48.8

¹ R_g from Guinier approximation.

² R_g from P(r) function.

³ Maximum intramolecular length, D_{max} .

⁴ Bayesian molecular mass, Mr, estimate and credibility interval with > 90% probability.

⁵ Hydrated particle volume (Porod volume) from regularized curve.

⁶ Mr from V_P .

^{7,8} Machine learning shape classification and Mr prediction, program DATCLASS.⁵¹

^{9,10} Volume and Mr of the *ab initio* models.

¹¹ Normalized Spatial Discrepancy of multiple *ab initio* reconstructions.

not free but mostly associated with ISCA2 to form a tight heterodimeric complex.⁶ This is consistent with *in vitro* data showing that purified apo ISCA1, once is mixed at a 1:1 ratio with purified apo ISCA2, is found fully and stably complexed with ISCA2.¹⁴ These data support that the formation of the ISCA1-ISCA2 complex *in vivo* stabilizes ISCA1 and prevents both proteins from their degradation. The latter aspect is consistent with an *in vivo* study on a pathogenic mutation of ISCA1, which showed that both ISCA1 and ISCA2 protein levels were diminished in the cells of the ISCA1 patient compared with control cells.³⁴

NFU1 elutes in a clear peak (Figure S2) with a stable R_g , yielding a SAXS curve with a good signal-to-noise by selecting the SEC frames at the tip of the peak. The estimate of the molar mass (Table 1) is in a good agreement with that of a NFU1 monomer. The dimensionless Kratky plot and P(r) function clearly indicate the presence of elongated species, and the modulations in the P(r) function suggest multiple domains (Figure S2). *Ab initio* models could be obtained ($\chi^2 \sim 1.1$ for all the 10 runs) with NSD value only slightly below 1, indicative of a certain variability of the reconstructions, which can be consistent with a protein with significantly flexible parts. The most representative model and the corresponding DAMMIF fit are shown in Figure 1A(2), 1B(2). Hybrid modelling was further performed by CORAL to visualize a plausible average conformation of apo NFU1. Ten CORAL runs (see Materials and Methods section for details) produced models with the fits in the range

$1.15 < \chi^2 < 1.51$, and a variety of conformations. The best fit and the corresponding structural model are shown in Figure 2A(2) and 2B(2), respectively. The generated models displayed variable bending of the N-terminal domain with respect to the C-terminal one about the linker and around the major molecular axis. The ten models are overlapped with the representative *ab initio* model in Figure S2. No inter-domain contacts were imposed on the CORAL modelling, as these contacts worsened fits leading to an underestimation of the scattering intensity at low angles. The present experimental data favour a relatively extended average conformation, without tight inter-domain contacts. Nevertheless, taken together, the results point to the need of explicitly addressing the molecular flexibility by describing the dominant conformations of apo NFU1 coexisting in solution and this was done using an Ensemble Optimization Method. Similar to the CORAL modelling, no inter-domain contacts were imposed, the two globular domains were connected through a random-coil type linker (12 residues), and completed with the flexible N- and C-terminal residues (see Materials and Methods section for details). The resulting R_g and D_{max} distributions are the average of 10 runs of the genetic algorithm applied to an initial pool of randomized 10,000 conformers. The best EOM fit and the distributions are shown in Figure 3A and 3B along representative compact and extended conformers. The distributions are clearly multimodal, with dominating medium-size and relatively compact conformations, but also a fat

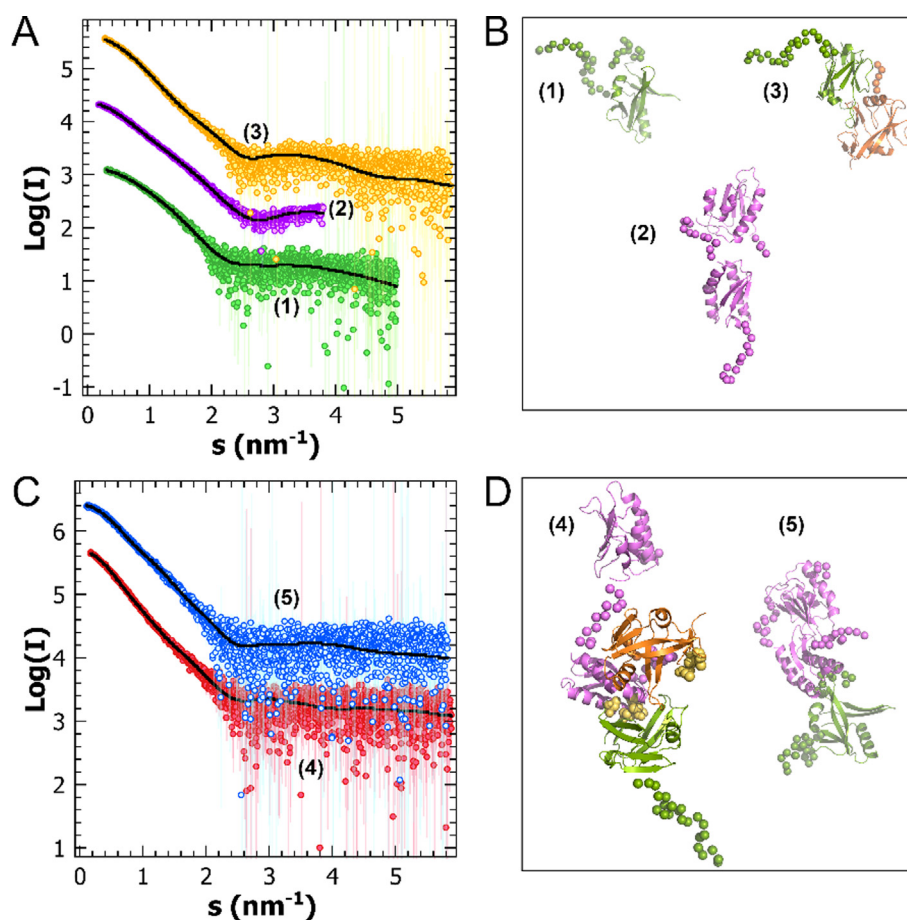


Figure 2. Hybrid modelling of [4Fe-4S] cluster binding proteins and complexes based on SAXS data. A. SAXS curves and best CORAL fit, of (1) apo ISCA1 (green), (2) apo NFU1 (magenta), (3) apo ISCA1(green)-ISCA2 (orange), vertically displaced for display. The corresponding models are shown in panel B. The C-terminal domain of NFU1 is invariably displayed as the bottom domain of the protein. Conformational heterogeneity is expected for NFU1 beyond the well-fitting CORAL model shown, representing an average conformation. C. SAXS curves and best CORAL fit of (4) apo ISCA1-ISCA2-NFU1 (ternary complex) and (5) apo ISCA1-NFU1 (binary complex), vertically displaced for display. The models of the complexes are shown in panel D with the same colour code of panel 2B. ISCA1 contacts NFU1 at the C-terminal domain and favours a compact conformation. ISCA1-ISCA2 is arranged such that ISCA2 is interposed between the C-terminal domain and the N-terminal domain of NFU1, favouring extended conformations. The conserved cysteine residues (Cys210 and Cys213 of NFU1, Cys57, Cys121 and Cys123 of ISCA1 and Cys79, Cys144 and Cys146 of ISCA2) are highlighted as yellow spheres in the ternary complex.

tail of extended conformers. Representative structures, which span the conformational (R_g , D_{max}) space of the selected ensembles were classified with DAMCLUST. This analysis shows that the dominant conformations are grouped in two clusters a compact and an extended one (see dummy atom averages and filtered models for the two clusters in Figure S2). The features of the representative conformations selected with EOM are presented in Figure 3C in the R_g , D_{max} space against the R_g , D_{max} pairs of the random pool, also highlighting the two main populations. The presence of compact and extended conformations agrees with previous NMR data which showed that the N- and C-domains, although displaying interdomain dynamic flexibility, are not fully

independent because they can recognize each other via specific hydrophobic and charged patches.⁵ Interestingly, the region 59–254 (corresponding to our construct) of the AlphaFold2³⁵ apo NFU1 structure, in which the globular domains are compacted very close to each other, gives a particularly bad fit ($\chi^2 = 77.2$, Figure S3), indicating that the AlphaFold2 model is excessively compact.

In summary, SAXS data indicated that a monomeric model with two disordered and flexible termini is preferable for apo ISCA1, thus indicating that the cluster binding region at the C-terminus containing two conserved Cys cluster ligands is highly dynamic and structurally disordered. A dynamic conformational behaviour is also present in monomeric apo NFU1, but this concerns the

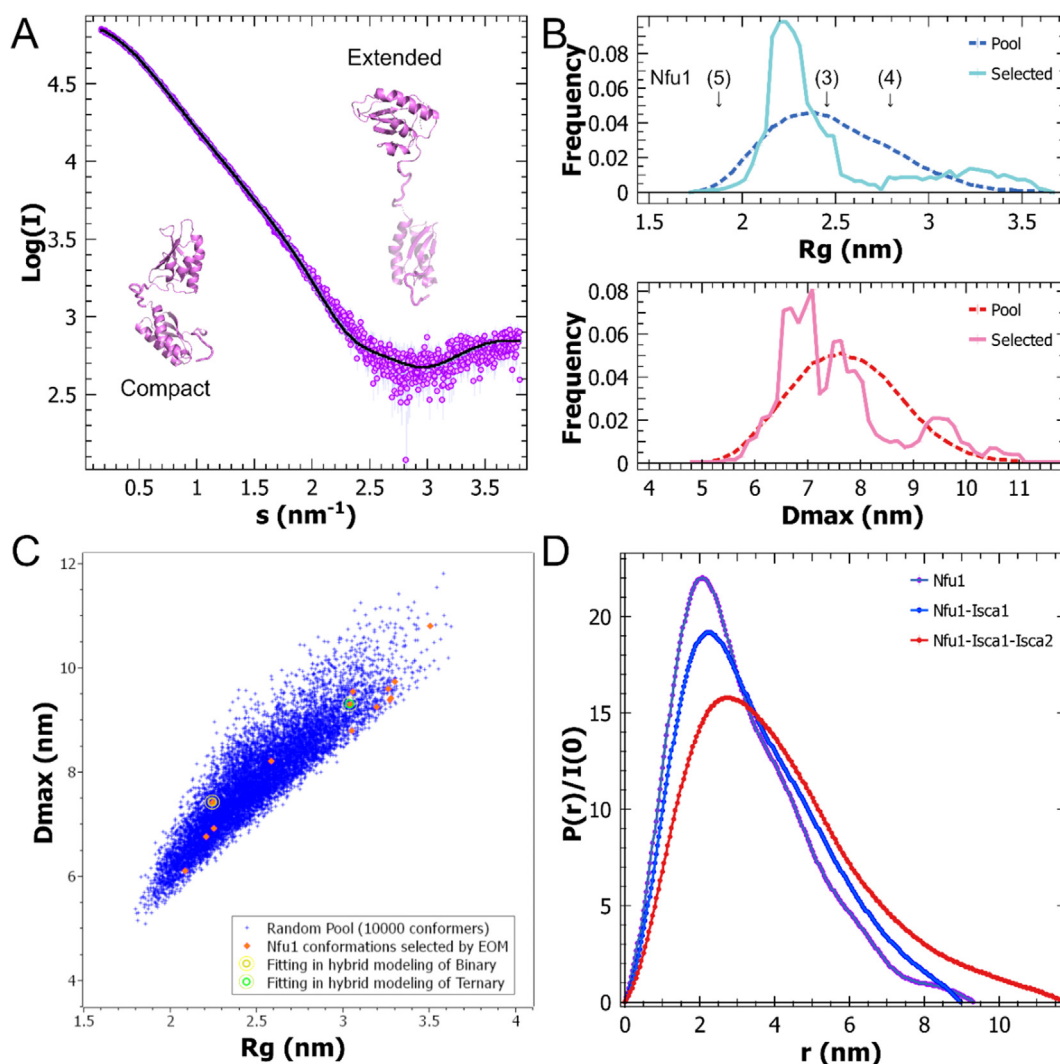


Figure 3. Conformational analysis of apo NFU1 by the Ensemble Optimization Method and comparison with model-free pair-distance distribution functions. A. EOM fit of SAXS data of apo NFU1. For the fit both compact and extended conformers of NFU1 are selected for the ensemble (NFU1 in representative conformations in the insets, C-terminal domain on the bottom). B. Radius of gyration (R_g , top) and maximum intramolecular length (D_{max} , bottom) distributions selected by EOM, in comparison with the distributions of a random pool of conformations. Above the R_g distributions, the arrows indicate the calculated R_g of NFU1 in models (3), (4), (5) of Figure 2 for comparison. C. Scatter plot of (R_g , D_{max}) pairs showing the conformational space of NFU1 compared to that of the random pool of conformers. The orange diamonds are the conformations highly populated in the EOM outputs. Two of those (highlighted) could be successfully used in an alternative CORAL modelling of the binary and ternary complexes. D. Comparison of the $P(r)$ functions, normalized by the forward scattering $I(0)$, for NFU1, the binary, and the ternary complex, showing that the binary complex has a similar D_{max} and the average cross-section to those of the apo NFU1, while the ternary complex is on average thicker, qualitatively supporting the suggested “interposition” mechanism for conformation change of NFU1 in the two complexes.

presence two dominant conformations in solution, a compact one having the N- and C-domains close in space and an extended one whose N- and C-domains are apart from each other.

Structural information on the apo ISCA1-ISCA2 complex by SEC-SAXS

In the mitochondrial NFU1-cluster acceptor pathway, the first complex that needs to be taken into account is the one formed by ISCA1 and

ISCA2 proteins. This complex is, indeed, the starting point of this pathway being in charge of assembling a $[4Fe-4S]^{2+}$ cluster with the assistance of IBA57 and of two electrons provided by the NADPH-FDXR-FDX2 chain.^{14,15} SEC-SAXS data were thus acquired on the apo ISCA1-ISCA2 complex and its structural modelling was obtained.

The apo ISCA1-ISCA2 complex eluted in two partially overlapping peaks (Figure S4). The

parameters in Table 1 indicated that the major peak at the higher elution volume is dominated by the monomeric apo ISCA1-ISCA2 complex, although again with a slight overestimation of molecular weight. A somewhat elongated shape is apparent from the maximum of the dimensionless Kratky plot and also manifests itself from a high- r tail of the $P(r)$ function (Figure S4). The modulations in the decaying part of the $P(r)$ function also suggest that the apo ISCA1-ISCA2 complex has an overall structure featuring multiple modules that can be visible at low resolution. Stable *ab initio* reconstructions were obtained for the complex, fitting the data with $\chi^2 \sim 1.2$ (Figure 1A(3) and 3B(3)). Ten independent shapes were analysed and the comparison of the averaged model with the most populated volume (using DAMAVER, Figure S4) reveals a conserved bent shape, with some variability around the edges. The SAXS data were further interpreted applying CORAL hybrid modelling. To this end, a structural model of the apo ISCA1-ISCA2 heterodimeric core was generated from the homodimeric *E. coli* SufA template (apo form, PDB code 2D2A³⁶), as described in the Materials and Methods section, being the C-terminal segments of both ISCA1 and ISCA2 in the ordered conformation, the one suited to bind a $[4\text{Fe-4S}]^{2+}$ cluster. In order to prevent excessive variability of the models between the repeated runs and, at the same time, to be able to fit the data satisfactorily, the interface between the subunits of the heterodimeric core was restrained setting contacts in CORAL between complementary residues, which are in the vicinity in the core model and are in agreement with a previous NMR study.¹⁴ In such a way, only some rearrangements between the two subunits of the heterodimeric core were allowed (see Materials and Methods section). Nine independent CORAL runs yielded satisfactory fits to the data with $\chi^2 = 1.13\text{--}1.42$. The best fit ($\chi^2 = 1.13$) and the corresponding structural model are shown in Figures 2A(3) and 3B(3), respectively, where the three Cys ligands for each of the two subunits of the heterodimer are solvent exposed on the opposite side of the dimer (*Cys-distant* structure, hereafter). The second best fit ($\chi^2 = 1.24$) shows a structure of the heterodimer where the three cysteine ligands face each other from the two subunits of the heterodimer (*Cys-close* structure, hereafter). Interestingly, this *Cys-close* structure mimics the ISCA1-ISCA2 structure obtained by AlphaFold multimer.³⁷ These results reproduce the same that were obtained on homodimeric ISCA2,²² and thus indicate that, at SAXS resolution of ~ 1 nm with the applied restraints between the subunit interfaces, two dimerization modes (*Cys-distant* and *Cys-close* structures) are plausible in the human apo ISCA2-ISCA1 heterodimer as well as in the ISCA2 homodimer. Both *Cys-distant* and *Cys-close* models of apo ISCA1-ISCA2 heterodimer overlap reasonably well with the *ab initio* reconstruction

whereby the disordered N-terminus of ISCA1 appears to protrude side-wise from the particle shape (Figure S4 shows a comparison of the *ab initio* model with the best CORAL model). The side-wise appearance of the ISCA1 N-terminus is conserved in all models, and is robust with respect to variations in the modelling choices (see Supplementary Data text and Figure S4). Alternative modelling further corroborates that the SufA-based template is the most appropriate (see Supplementary Data text).

In summary, SAXS data are consistent with a heterodimeric apo ISCA1-ISCA2 complex having a dimerization interface similar to that present in *E. coli* SufA and in human ISCA2 homodimers. In addition, the SAXS data can be nicely fitted with the C-terminal segments of both ISCA1 and ISCA2 being structurally ordered. In this ordered structural arrangement, the three cysteine ligands can face each other from the two ISCA1 and ISCA2 subunits of the heterodimer (*Cys-close* structure), in such a way allowing the assembly of the $[4\text{Fe-4S}]^{2+}$ cluster at the subunit-subunit interface of the apo ISCA1-ISCA2 heterodimer, or can be solvent exposed on the opposite side of the dimer (*Cys-distant* structure), in order to share the $[4\text{Fe-4S}]^{2+}$ cluster binding with other partners.

Structural information on the apo ISCA1-ISCA2-NFU1 ternary complex by SEC-SAXS

Once the $[4\text{Fe-4S}]^{2+}$ cluster is assembled on the ISCA1-ISCA2 complex, NFU1 protein takes part to the $[4\text{Fe-4S}]^{2+}$ cluster trafficking in the mitochondrial NFU1-cluster acceptor pathway.⁸ A specific interaction of the C-domain of NFU1 with ISCA1, the latter still complexed with ISCA2, occurs indeed to form a ISCA1-ISCA2-NFU1 ternary complex.²⁸ To structurally investigate this step, SEC-SAXS data were acquired on a sample containing the apo ISCA1-ISCA2-NFU1 complex. Despite the elution of the sample showing shoulders and satellite peaks (Figure S5A), the SAXS curve from the most prominent peak displays overall parameters close to the ones expected for a ternary complex. The data can then be considered representatives of the apo ISCA1-ISCA2-NFU1 complex. The overall parameters of the SAXS profile presented in Table 1 are compatible with the formation of a ternary complex. Importantly, the SAXS data are not representative of a simple mixture without association, as they cannot be satisfactorily fitted by a linear combination of the experimental scattering intensities of the complex components (apo NFU1 and apo ISCA1-ISCA2). This further corroborates the identification of the ternary complex as belonging to the SAXS profile (misfits not shown). As first step, ten *ab initio* DAMMIF reconstructions of the SAXS curve of the ternary complex were performed, yielding good fits with $\chi^2 \sim 1.1$ (see Figure 1A(4) and 1B(4)). The model shows that the ternary apo ISCA1-ISCA2-NFU1 complex is elongated and it features a

clear protruding lobe at the centre. Second, the apo ISCA1-ISCA2-NFU1 complex can be approached using hybrid modelling in CORAL to obtain the average conformations of this complex, with a similar approach as used for the SAXS-based structural modelling of isolated apo NFU1 and apo ISCA1-ISCA2 (see Materials and Methods). Ten CORAL runs for the ternary complex resulted in solutions (χ^2 in the range 1.13–1.45) with the best fit and the corresponding structural model shown in Figure 2C(4) and 2D(4), respectively. The best model displays ISCA2 in the lobe at the center and ISCA1 external to NFU1, and shows a *Cys-distant* structure-like arrangement of the ISCA1-ISCA2 heterodimer, i.e. with the three Cys ligands for each of the two subunits on the opposite side of the heterodimer, and with Cys residues of ISCA1 close to Cys residues of NFU1, while those of ISCA2 far from them. It is evident that, in this case, NFU1 is locked in an extended conformation by interposition of ISCA2. There is, however, some heterogeneity in the *Cys-distant* structure-like arrangement not confined to the flexible termini and linkers, as 50% of the modelled structures feature ISCA1 in position of ISCA2 and vice-versa, as these are relatively similar at the SAXS resolution and the deviations from the contact constraints with the NFU1 C-terminal domain are small. Nevertheless, the best fit and second best fit are arranged as in Figure 2D(4), i.e. placing ISCA1 Cys ligands in close contact with the C-domain of NFU1 while those of ISCA2 far from it. This structural arrangement also fits well with previous NMR data, which indicated that the Cys ligands of ISCA1 are close to the CXXC motif of the C-domain of NFU1 to bridge the $[4\text{Fe-4S}]^{2+}$ cluster with ISCA1.²⁸ Last but not least, the same position of ISCA1 external to NFU1 is also maintained in the ISCA1-NFU1 binary complex (see later). For all these reasons, we consider the configuration reported in Figure 2D(4) is the most realistic to mimic the binding of a $[4\text{Fe-4S}]^{2+}$ cluster bridged between ISCA1 and NFU1.

In summary, SAXS data in combination with available high-resolution NMR information²⁸ indicate that, in the ternary apo ISCA1-ISCA2-NFU1 complex, NFU1 assumes a unique extended conformation due to the interposition of ISCA2, and that a *Cys-distant* structure-like arrangement of the ISCA1-ISCA2 heterodimer is likely privileged with respect to a *Cys-close* structure. This structural model fits well with a $[4\text{Fe-4S}]^{2+}$ cluster bridged between ISCA1 and NFU1 in the ternary complex, in agreement with what was previously shown by us in a study where a $[4\text{Fe-4S}]$ ISCA1-ISCA2 complex was mixed with apo NFU1.²⁸

Structural information on the apo ISCA1-NFU1 binary complex by SEC-SAXS

The ternary ISCA1-ISCA2-NFU1 complex is an intermediate of the mitochondrial NFU1-cluster acceptor pathway as it evolves to form the binary

ISCA1-NFU1 complex once the $[4\text{Fe-4S}]^{2+}$ cluster in the ternary complex is mobilized from the ISCA1-ISCA2 cluster-assembly site to the ISCA1-NFU1 cluster-transfer site.²⁸ On this basis, we have here structurally investigated by SEC-SAXS a sample containing the apo ISCA1-NFU1 complex. The elution of the sample shows an intense main peak (Figure S5B), whose SAXS curve displays overall parameters close to the ones expected for a binary complex (Table 1), and again it cannot be well fitted as a simple mixture of apo ISCA1 and apo NFU1 (misfits not shown). The data can therefore be considered representatives of the apo ISCA1-NFU1 complex. Moreover, the volumes evaluated from the SAXS curve, smaller than the sum of the volumes of apo ISCA1 and apo NFU1 may suggest a structural rearrangement of NFU1 upon ISCA1 interaction. Comparing in Figure 3D the $I(0)$ -normalized $P(r)$ function of the apo ISCA1-NFU1 complex with those of isolated apo NFU1 and of the ternary apo ISCA1-ISCA2-NFU1 complex, it results that qualitatively the binary complex must have a typical thickness (related to the position of the maximum of $P(r)$ functions) smaller than the ternary complex, and only slightly larger than apo NFU1. The shape of the $P(r)$ functions indicates that all these constructs are elongated, but with the maximum length of the binary complex and apo NFU1 being comparable and the ternary complex being longer.

Ten *ab initio* DAMMIF reconstructions were performed, yielding good fits with $\chi^2 \sim 1.1$ (see Figure 1A(5) and 1B(5)). In agreement with the qualitative $P(r)$ function analysis described above, the models demonstrate that the binary apo ISCA1-NFU1 complex is less elongated than the ternary apo ISCA1-ISCA2-NFU1 complex, and with no lobe at the centre at variance of what present in the ternary complex. Again, a hybrid modelling approach was applied to obtain the average conformations of the apo ISCA1-NFU1 complex. Ten CORAL runs for the binary complex resulted in models with good agreement with the data (χ^2 varying from 1.07 to 1.46), and all with a similar arrangement of the domains (the best fit and the corresponding structural model are shown in Figure 2C(5) and 2D(5), respectively). Here, NFU1 is in a particularly compact conformation at variance with the extended conformation found in the ternary ISCA1-ISCA2-NFU1 apo complex, and ISCA1 associates distally to the C-terminal domain of NFU1, at a similar position as in the best fit for the ternary complex. The values of R_g in the best CORAL reconstruction of apo NFU1, and calculated for the NFU1 subunit in the context of apo ISCA1-NFU1 and apo ISCA1-ISCA2-NFU1 CORAL models with fully flexible termini and linkers shown in Figure 2, are marked in Figure 3B. They show that the apo NFU1 CORAL model represents an average conformation, while, in the apo ISCA1-ISCA2-NFU1 complex, NFU1 is

in an extended conformation and, in the apo ISCA1-NFU1 complex, NFU1 is in a very compact conformation. In [Figure 3C](#), the R_g , D_{max} pair for the conformers selected for the CORAL modelling with rigid NFU1 is highlighted against the conformational R_g , D_{max} space of the EOM random pool, showing that the interactions of NFU1 in the binary complex selects compact conformers of NFU1 and the interactions of NFU1 in the ternary complex select extended conformations. Further consistency checks with the SAXS data on the different conformations of NFU1 present in the binary vs. ternary complex are reported in the [Supplementary Data](#) text.

In summary, the SAXS data allowed us to propose that, in the case of apo ISCA1-NFU1, a compact conformer of NFU1 participates in the complex formation, at variance with what observed for apo ISCA1-ISCA2-NFU1, where the placement of ISCA2 in the middle of the complex forces an extended conformation for NFU1. The dynamic modular domain organization of NFU1 is thus nicely designed to select different protein partnerships.

[4Fe-4S]²⁺ cluster coordination in the ISCA1-NFU1 complex

Previous paramagnetic NMR data showed that both ISCA1-ISCA2-NFU1 and ISCA1-NFU1 complexes bind the [4Fe-4S]²⁺ cluster with ligands of the same nature, which bridge the cluster between ISCA1 and NFU1.²⁸ The ligands typical of [4Fe-4S] clusters are Cys residues. NFU1 contains only two Cys residues (the conserved Cys210 and Cys213), while ISCA1 contains three Cys residues (the conserved Cys57, Cys121 and Cys123). Thus, we expect that the [4Fe-4S]²⁺ cluster in the heterodimeric ISCA1-NFU1 complex is coordinated by four Cys residues out of the five Cys available. However, which are the cysteines coordinating the cluster among Cys210 and Cys213 of NFU1 and Cys57, Cys121 and Cys123 of ISCA1 is still not defined. Thus, we have here characterized [4Fe-4S]²⁺ cluster ligand coordination on the ISCA1-NFU1 complex via a site-directed mutagenesis-spectroscopic combined approach. This characterization also provides the cluster ligand coordination on the ISCA1-ISCA2-NFU1 complex. The Cys residues in NFU1 and ISCA1 were mutated to Ala to abolish their cluster binding abilities. Cys210Ala and Cys213Ala single mutants of NFU1, Cys57Ala, Cys121Ala and Cys123Ala single mutants of ISCA1 and a Cys121Ala/Cys123Ala double mutant of ISCA1 were produced (see Materials and Methods for details). The individual apo ISCA1-NFU1 complexes were generated and then each was chemically reconstituted following the same procedure applied to the wild-type apo ISCA1-NFU1 complex (see Materials and Methods for details).

UV-visible spectra of the mutated, chemically reconstituted ISCA1-NFU1 complexes were recorded in order to monitor Fe-S cluster binding. It resulted that no UV-visible bands typically characterizing Fe-S cluster binding were observed in the spectra of both ISCA1-Cys210Ala NFU1 and ISCA1-Cys213Ala NFU1 complexes, indicating that the cysteines of the CXXC motif of NFU1 are absolutely required as ligands to bind the [4Fe-4S]²⁺ cluster in the wild-type ISCA1-NFU1 complex. On the contrary, UV-visible bands are observed for the complexes involving the single and double mutants of ISCA1. Specifically, a broad band centered at ~410 nm, which typically dominates the absorption spectra of biological [4Fe-4S]²⁺ clusters,³⁸ is observed for all complexes and is the same as that observed for the wild-type [4Fe-4S]²⁺ ISCA1-NFU1 complex ([Figure 4A](#)). The intensity of the band at ~410 nm is, however, different comparing the UV-visible spectra of the Cys-mutated ISCA1-NFU1 complexes with that of wild-type complex. This band has a lower intensity in the ISCA1 mutated-NFU1 complexes with respect to that of wild-type complex, although at a different extent, indicating that the removal of one or two Cys residues negatively affects the fraction of bound [4Fe-4S]²⁺ cluster. In particular, the ISCA1-NFU1 complex involving the double Cys121Ala/Cys123Ala mutant of ISCA1 results poorly metallated, while a single mutation of ISCA1 cysteines have a minor effect on the metalation level of the ISCA1-NFU1 complex ([Figure 4A](#)). These data indicate that, at variance with ISCA1-Cys mutated NFU1 complexes, the single and double mutations of cysteines in ISCA1 does not abolish the [4Fe-4S]²⁺ cluster binding in the ISCA1-NFU1 complex, although they reduce the [4Fe-4S]²⁺ cluster bound levels. These results are consistent with the quantification of the iron and acid-labile sulfide ion content obtained on these chemically reconstituted samples. Indeed, these analyses indicate that, while the wild-type complex binds ~ 1 [4Fe-4S] cluster per heterodimer, the single ISCA1 mutated complexes binds slightly lower amounts of [4Fe-4S] cluster per heterodimer ranging from 0.8 to 0.9 and the double ISCA1 mutated complex binds the lowest amount of [4Fe-4S] cluster, i.e. ~ 0.45 ([Figure S6](#)).

From the UV-visible data analysis described above, we concluded that Cys210 and Cys213 of NFU1 are two ligands of the [4Fe-4S]²⁺ cluster in the wild-type ISCA1-NFU1 complex. Now, in order to identify the two other [4Fe-4S]²⁺ cluster ligands in the dimeric hetero-complex that necessarily belong to ISCA1 (NFU1 does not contain indeed any other [4Fe-4S]²⁺ cluster Cys ligands, besides Cys210 and Cys213), paramagnetic 1D ¹H NMR spectra were recorded on four dimeric hetero-complexes formed by a subunit of native NFU1 and a subunit of Cys-mutated ISCA1 (Cys57Ala ISCA1, Cys121Ala/Cys123Ala ISCA1, Cys121Ala

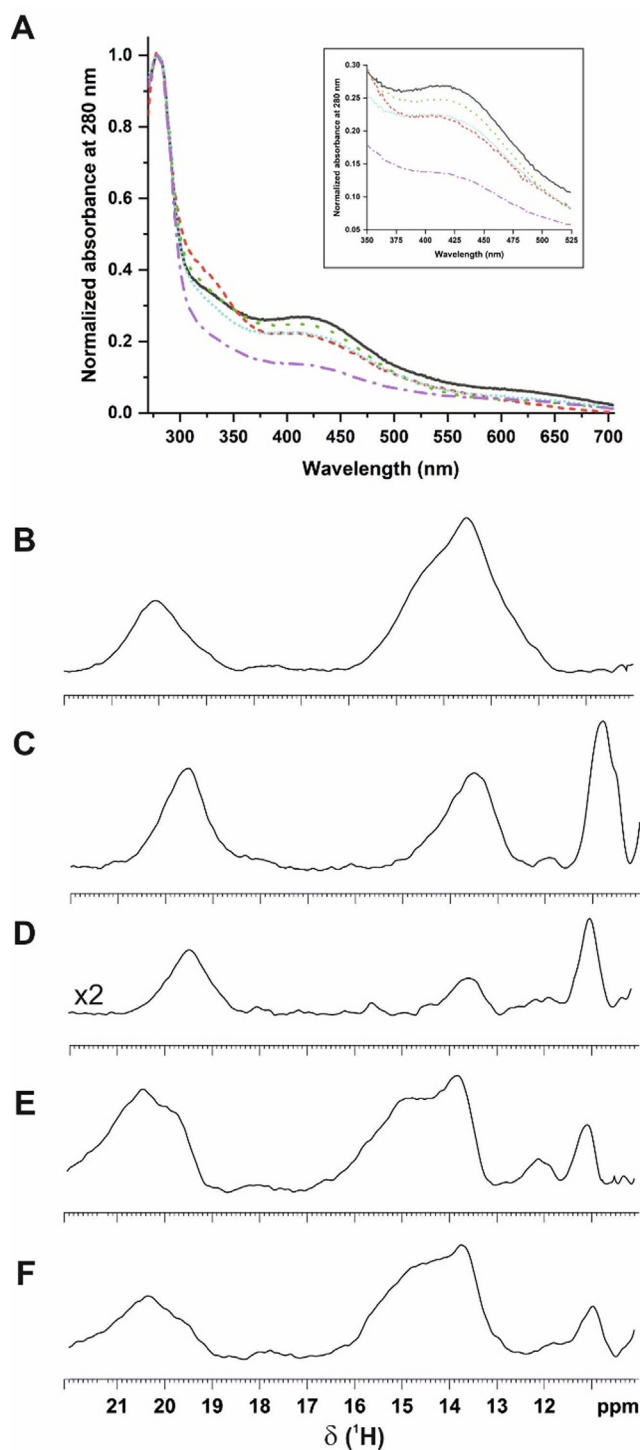


Figure 4. Characterization of [4Fe-4S] cluster binding in ISCA1-NFU1 complex by UV-visible and paramagnetic NMR spectroscopies. A. Normalized UV-visible absorption spectra at 280 nm of chemically reconstituted [4Fe-4S]²⁺ ISCA1-NFU1 wild-type and Cys → Ala mutated complexes wild-type ISCA1-NFU1 complex (black), Cys57Ala ISCA1-NFU1 complex (red short dash), Cys121Ala ISCA1-NFU1 complex (green dot), Cys123Ala ISCA1-NFU1 complex (cyan short dot) and Cys121Ala/Cys123Ala ISCA1-NFU1 complex (purple dash dot). 1D ¹H paramagnetic NMR spectra acquired at 298 K on B. [4Fe-4S]²⁺ Cys57Ala ISCA1-NFU1 complex C. [4Fe-4S]²⁺ wild-type ISCA1-NFU1 complex D. [4Fe-4S]²⁺ Cys121Ala/Cys123Ala ISCA1-NFU1 complex E. [4Fe-4S]²⁺ Cys121Ala ISCA1-NFU1 complex F. [4Fe-4S]²⁺ Cys123Ala ISCA1-NFU1 complex. x2 indicates that the intensity of the spectrum has been scaled to equalize the noise level for a better comparison of the signals.

and Cys123Ala). They were then compared to that of the wild-type complex. For all chemically reconstituted complexes, the 1D ^1H NMR spectra (Figure 4B-F) showed that the chemical shift values of the paramagnetic signals, their anti-Curie temperature dependence, and their linewidths, are typical of $\text{H}\beta$ signals of Cys residues bound to a $[\text{4Fe-4S}]^{2+}$ cluster with an $S = 0$ electronic spin ground state, with the paramagnetism arising from excited states of the electron spin ladder, partially populated at room temperature.^{39–41} All the observed NMR signals can be thus assigned to the $\text{H}\beta$ protons of cysteine ligands bound to a $[\text{4Fe-4S}]^{2+}$ cluster. The chemical shifts of the $\text{H}\beta$ protons for the four Cys mutated ISCA1-NFU1 complexes do not differ significantly from those of the wild-type ISCA1-NFU1 complex (Figure 4B-F). We observed indeed that the paramagnetic signals have chemical shifts in the same ppm region. This is because the Cys to Ala mutations do not alter the +2 redox state of the $[\text{4Fe-4S}]^{2+}$ cluster as well as its nuclearity. Only upon Fe-S cluster redox and nuclearity changes, we expect indeed large variations of the chemical shifts.³⁹ On the contrary, the chemical shift range, typically observed for the $\text{H}\beta$ protons of the cysteines bound to a $[\text{4Fe-4S}]^{2+}$ cluster, is not largely affected by the modifications of the coordination sphere obtained by Cys ligand removal⁴⁰ or by Cys ligand substitution.⁴²

The paramagnetic 1D ^1H NMR spectrum of $[\text{4Fe-4S}]^{2+}$ Cys57Ala ISCA1-NFU1 complex shows a signal centered at 20.2 ppm and two close signals at 14.5 and 13.7 ppm (Figure 4B). The signals at 20.2 and 13.7 ppm are also present in the 1D ^1H NMR spectrum of the wild-type $[\text{4Fe-4S}]^{2+}$ ISCA1-NFU1 complex with small chemical shift variations, while the signal at 10.8 ppm is present only in the wild-type complex and the new signal at 14.5 ppm is present only in the 1D ^1H NMR spectrum of the $[\text{4Fe-4S}]^{2+}$ Cys57Ala ISCA1-NFU1 complex (Figure 4B and 4C). These results can be interpreted as follows: i) since we showed that Cys residues of NFU1 are absolutely required to bind the $[\text{4Fe-4S}]^{2+}$ cluster in the ISCA1-NFU1 complex, the two signals at 20.2 and 13.7 ppm that are present in both spectra of wild-type and Cys57Ala ISCA1-NFU1 complex can be assigned to the $\text{H}\beta$ protons of Cys210 and Cys213 of NFU1; ii) the signal at 10.8 ppm, which disappears upon Cys57 mutation in the 1D ^1H NMR spectrum of the $[\text{4Fe-4S}]^{2+}$ Cys57Ala ISCA1-NFU1 complex, can be assigned to a $\text{H}\beta$ proton of Cys57 of ISCA1; iii) the new signal at 14.5 ppm can be assigned to a $\text{H}\beta$ proton of a ligand of ISCA1 coordinating the cluster only upon Cys57 mutation. On this basis, we can conclude that Cys57 is the third ligand in the wild-type $[\text{4Fe-4S}]^{2+}$ ISCA1-NFU1 complex, and that Cys57 can be replaced by Cys121 or 123 of ISCA1 in the $[\text{4Fe-4S}]^{2+}$ Cys57Ala ISCA1-NFU1 complex,

which thus result both involved in cluster coordination in the latter complex. Comparing the 1D ^1H NMR spectrum of $[\text{4Fe-4S}]^{2+}$ Cys121Ala/Cys123Ala ISCA1-NFU1 complex with that of the wild-type $[\text{4Fe-4S}]^{2+}$ ISCA1-NFU1 complex (respectively, Figure 4D vs. 4C), it results that the signals at 19.5, 10.8 and 13.5 ppm present in the wild-type complex are also present in the $[\text{4Fe-4S}]^{2+}$ Cys121Ala/Cys123Ala ISCA1-NFU1 complex but with relative intensities different from the those observed in the wild-type complex. This finding suggests the occurrence of populations with different coordination environments in the latter double mutated complex. The 1D ^1H NMR spectra of the other two $[\text{4Fe-4S}]^{2+}$ ISCA1-NFU1 complexes involving the single Cys121Ala and Cys123Ala mutations display more signals with respect to those typically observed in the 20–10 ppm region, i.e. four signals assigned to four $\text{H}\beta$ protons of four Cys ligands of a $[\text{4Fe-4S}]^{2+}$ cluster⁴¹ (Figure 4E and 4F). This again suggests the presence of various species with different coordination environments, which is likely originated, as suggested for the $[\text{4Fe-4S}]^{2+}$ Cys57Ala ISCA1-NFU1 complex, by the possibility that the Cys of ISCA1 next to the mutated one become an additional ligand, supporting that Cys121 and Cys123 can swap in cluster binding.

Overall, these data support a model where, in both ISCA1-ISCA2-NFU1 and ISCA1-NFU1 wild-type complexes, Cys210 and Cys213 of NFU1 and Cys57 of ISCA1 coordinate three iron atoms of the $[\text{4Fe-4S}]^{2+}$ cluster, and that the fourth ligands can involve either Cys121 or Cys123.

Discussion

Based on *in vivo* and proteomics data, multiple pathways have been proposed to be active for the assembly and trafficking of $[\text{4Fe-4S}]$ clusters in human mitochondria.^{6,7,9} Two main pathways have been proposed to operate under physiological conditions depending on by whom the $[\text{4Fe-4S}]^{2+}$ cluster is assembled. In a pathway (the NFU1-cluster acceptor pathway), two homologous proteins belonging to ISCA protein family, i.e. ISCA1-ISCA2, act as a platform to assemble a $[\text{4Fe-4S}]^{2+}$ cluster on a heterodimeric ISCA1-ISCA2 complex with the assistance of the electron donor FDX2 and the IBA57 protein, whose molecular role in the process is still not defined.^{14,15} In this pathway, the accessory protein NFU1 acts downstream the ISCA1-ISCA2 complex receiving the $[\text{4Fe-4S}]^{2+}$ cluster assembled on the ISCA1-ISCA2 complex and then transferring it to mitochondrial apo recipient proteins.^{28,30} In the other pathway, $[\text{2Fe-2S}]^{2+}$ cluster-bound forms of ISCA1 and ISCU2 interact with dimeric NFU1 to donate their clusters, which then reductively couple into a $[\text{4Fe-4S}]^{2+}$ cluster upon the provision of two electrons by the electron donor FDX2.⁹ In this pathway, dimeric NFU1 works

as the platform to assemble a $[4\text{Fe-4S}]^{2+}$ cluster bypassing the formation of the ISCA1-ISCA2 complex, which is, on the contrary, the complex indispensable in the mitochondrial NFU1-cluster acceptor pathway to assemble a $[4\text{Fe-4S}]^{2+}$ cluster. The multi-protein complex composed by ISCA1, ISCU2, FDX2 and dimeric $[4\text{Fe-4S}]^{2+}$ NFU1 was also proposed to interact with mitochondrial apo recipient proteins to transfer to them the assembled $[4\text{Fe-4S}]^{2+}$ cluster.⁹

Here, we focused our attention on the $[4\text{Fe-4S}]^{2+}$ cluster transfer mechanism acting in the mitochondrial NFU1-cluster acceptor pathway. This is a complex process, in which detailed structural information are missing. This gap originates from the fact that transient and dynamic protein-protein interaction events occur among the various involved proteins. Hence, these highly dynamic molecular events occurring along the $[4\text{Fe-4S}]^{2+}$ cluster transfer pathway make the typical structural techniques including X-ray crystallography, NMR spectroscopy, and electron microscopy quite challenging to succeed with a high-resolution structure determination. Here, we faced this molecular complexity via an approach that integrate small-angle X-ray scattering coupled with on-line size-exclusion chromatography³¹ and NMR. This approach, although providing structural information at low resolution, is ideally suitable for structural modelling of these highly dynamic systems.

Our study provides a structural view of how ISCA1, ISCA2 and NFU1 coordinate, along the mitochondrial NFU1-cluster acceptor pathway, their interactions to safely direct $[4\text{Fe-4S}]^{2+}$ clusters towards mitochondrial apo recipient proteins. This information also provides a first rationale at the molecular level for the function of the N-domain of NFU1. Specifically, we were able to obtain the most plausible structural models of ternary and binary complexes involving ISCA1, ISCA2 and NFU1 proteins, which are consistent with the solution scattering and with the contacts between the subunits of the complexes derived from experimental NMR data available in the literature.^{14,28} These structural models allowed us to unravel how intra- and inter-molecular interaction events occurring between ISCA1, ISCA2 and NFU1 modulate the quaternary structure of the formed complexes to safely guide $[4\text{Fe-4S}]^{2+}$ cluster transfer. Our study focused on the interactions between the apo proteins because the $[4\text{Fe-4S}]^{2+}$ cluster is transiently shared among the ISCA1, ISCA2 and NFU1 interacting proteins. Indeed, the $[4\text{Fe-4S}]^{2+}$ cluster rapidly flows from cluster-assembly site of ISCA1-ISCA2 to the cluster-transfer site of ISCA1-NFU1 upon mixing $[4\text{Fe-4S}]^{2+}$ ISCA1-ISCA2 complex with apo NFU1, with no stable cluster-intermediates spectroscopically observable.²⁸ Nevertheless, the here described change of the quaternary structure arrangement in the apo complexes

still provide relevant information on how the $[4\text{Fe-4S}]^{2+}$ cluster can be mobilized, as described hereafter.

First, SEC-SAXS data analysis showed that apo NFU1 is a monomer displaying a high dynamic conformational behaviour with the presence two dominant conformations in solution, a compact one having the N- and C-domains close in space and an extended one whose N- and C-domains are far apart from each other. The extended conformation can definitely involve the two cysteine residues in $[4\text{Fe-4S}]^{2+}$ cluster binding since they are structurally exposed to the solvent in the C-terminal domain of NFU1. However, also the compact conformation shows that the two cysteine residues are far away from the domain-domain interacting region and thus still result highly solvent exposed. Therefore, also in the compact conformation, the two cysteine residues can bind a $[4\text{Fe-4S}]^{2+}$ cluster.

Second, we showed that SEC-SAXS data of apo ISCA1-ISCA2 hetero-complex allow interpretations featuring some variability at the heterodimeric interface, analogously to what we previously reported for homodimeric apo ISCA2.²² Two dimerization modes are, indeed, possible: one, corresponding to the best fit, exposing the cysteine of the two subunits on the opposite sides (*Cys-distant* structure), the other, the second best fit, facing the cysteines of the two subunits (*Cys-close* structure). In the *Cys-close* structure, ISCA1 and ISCA2 subunits approaches the cysteines of the two CX₆₃(or₆₄)CXC motifs required for the $[4\text{Fe-4S}]^{2+}$ cluster-assembly (Figure 5A). On the other hand, the *Cys-distant* structure of the ISCA1-ISCA2 complex allows sharing the $[4\text{Fe-4S}]^{2+}$ cluster with its partner, i.e. the C-domain of NFU1 (Figure 5A). The same *Cys-distant/close* structural variability has been also observed in ISCA2 homodimer as well as upon its interaction with IBA57 to share a $[2\text{Fe-2S}]$ cluster.²²

The two conformations of apo NFU1 (extended and compact) and the potential structural plasticity of the ISCA1-ISCA2 heterodimer (*Cys-close* and *Cys-distant* structures) can play a crucial role to properly activate $[4\text{Fe-4S}]^{2+}$ cluster transfer towards mitochondrial final targets. We showed, indeed, that apo NFU1 is locked in an extended conformation upon the ternary complex formation between apo NFU1 and the heterodimeric apo ISCA1-ISCA2 complex (Figure 5B). The structural model of the ternary (ISCA1-ISCA2-NFU1) apo complex shown in Figure 5A is consistent with the binding of a $[4\text{Fe-4S}]^{2+}$ cluster shared by CXXC motif of C-domain of NFU1 and CX₆₃CXC motif of ISCA1. In the best model obtained for the ternary complex, the ISCA2 subunit interacts with the ISCA1 subunit exposing its own CX₆₄CXC motif far away from that of ISCA1, thus avoiding a $[4\text{Fe-4S}]^{2+}$ cluster binding bridged between the two ISCA subunits. The extended conformation of

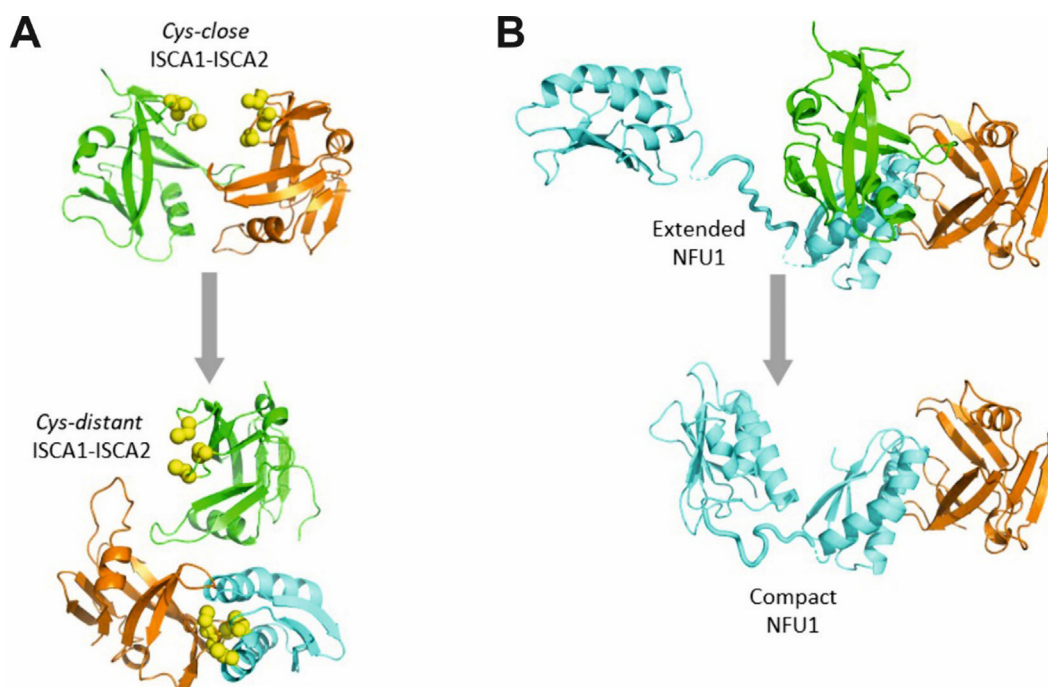


Figure 5. Association changes of ISCA1, ISCA2 and NFU1 proteins proposed to occur in promoting $[4\text{Fe-4S}]$ cluster transfer. Structural low-resolution models of ISCA1-ISC2, ISCA1-ISC2-NFU1 and ISCA1-NFU1 apo complexes obtained by SEC-SAXS data. ISCA1 is in orange, ISCA2 in green and NFU1 in cyan, side-chains of cysteine residues are showed as yellow spheres. A. ISCA1-ISC2 apo complex is in a Cys-close structural arrangement with the three conserved cysteine facing each other from the two subunits of the heterodimer to assembly a $[4\text{Fe-4S}]^{2+}$ cluster. In the ISCA1-ISC2-NFU1 apo complex, ISCA1-ISC2 proteins are in a Cys-distant structural arrangement, where ISCA2 exposes its conserved Cys residues far away from those of ISCA1. The C-domain of NFU1 (here shown) tightly interacts with ISCA1 with its CXXC motif close to the conserved cysteine CX_{63}CXC motif of ISCA1 to bridge a $[4\text{Fe-4S}]^{2+}$ cluster. B. The extended and compact conformations of NFU1 obtained shifting from the ternary ISCA1-ISC2-NFU1 apo complex to the binary ISCA1-NFU1 apo complex upon the release of ISCA2.

NFU1 is a consequence of the position of ISCA2 subunit in the ternary complex. ISCA2 subunit prevents, indeed, the N-domain of NFU1 to stay positioned close the C-domain to form a compact conformation. We can speculate that the Cys-close ISCA1-ISC2 complex specifically selects the extended conformation of NFU1 to trigger the mobilization of the $[4\text{Fe-4S}]^{2+}$ cluster from the cluster-assembly site formed by the ISCA1-ISC2 complex to the cluster-transfer site formed by ISCA1-NFU1 complex. Such $[4\text{Fe-4S}]^{2+}$ cluster transfer can promote a switch of ISCA1-ISC2 complex from the Cys-close to the Cys-distant structure (Figure 6). According to this model, while the ISCA2 subunit is located in a protruding lobe of the ternary complex with a limited number of interactions with NFU1, the ISCA1 subunit tightly interacts with the C-domain of NFU1. The tight interaction between ISCA1 and NFU1 in the ternary complex might be the requisite to switch ISCA1-ISC2 Cys-close structure into ISCA1-ISC2 Cys-distant structure in order to transfer the $[4\text{Fe-4S}]^{2+}$ cluster from the assembly site located at the subunit-subunit interface of ISCA1

and ISCA2 to the binding site formed by ISCA1 and NFU1 (Figure 6).

Once the $[4\text{Fe-4S}]^{2+}$ cluster transfer step occurred in the ternary complex, the ISCA2 subunit is no more cluster-bridged with ISCA1 and thus displays a weaker interaction with ISCA1. The latter, on the contrary, bridges the $[4\text{Fe-4S}]^{2+}$ cluster with the C-domain of NFU1 strengthening the ISCA1-NFU1 interaction. These effects can favour the release of ISCA2 from the ternary complex to form the binary ISCA1-NFU1 complex (Figure 6). This is in agreement with what has been previously documented by analytical gel filtration data that showed indeed the presence of an equilibrium between the ternary and binary complexes.²⁸ At variance with the ternary complex, NFU1 in the formed binary apo ISCA1-NFU1 complex is locked in a compact conformation where ISCA1 assumes the same position found in the ternary complex (i.e. interacting with the C-domain of NFU1), while the N-domain of NFU1 replaces the ISCA2 position (Figure 5B). So, the release of ISCA2 can allow the N-domain of NFU1 to fix the compact conformation at the expenses of the

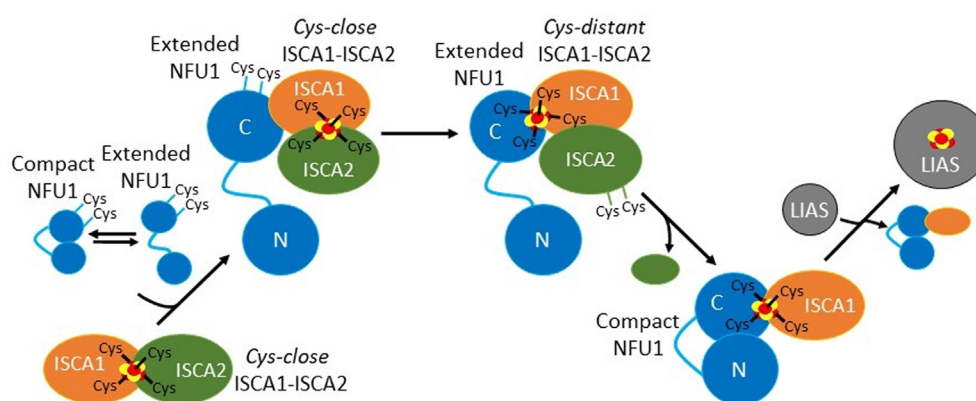


Figure 6. Molecular model of the protein–protein interactions driving [4Fe-4S] cluster from ISCA1-ISCA2 complex to the mitochondrial apo recipient protein LIAS. The [4Fe-4S]²⁺ ISCA1-ISCA2 complex in a Cys-close structural arrangement selects the extended conformation of NFU1 to form a ternary complex in which the [4Fe-4S]²⁺ cluster shifts from the assembly site located at the subunit-subunit interface of ISCA1 and ISCA2 to the binding site formed by ISCA1 and NFU1 interaction. In the latter state, ISCA1 and ISCA2 proteins are in a Cys-distant structural arrangement. Upon the release of ISCA2, a binary ISCA1-NFU1 complex bridging the [4Fe-4S]²⁺ cluster via the CXXC motif of NFU1, Cys57 and Cys121 or Cys123 of ISCA1 and where NFU1 takes a compact conformation is formed. The binary complex has been shown to be able to insert the [4Fe-4S]²⁺ cluster into LIAS.³⁰

extended conformation of NFU1, thus protecting the [4Fe-4S]²⁺ cluster. We noticed that the structures predicted using AlphaFold2 multimer³⁷ maintain, both for the binary and ternary complexes, a very compact conformation for the flexible NFU1. These structures result in a worse fit to the SAXS data than the present modelling (Figure S3), indicating that the predicted NFU1 structure in the AlphaFold2 binary and ternary models is excessively compact.

We showed here that both extended and compact NFU1 conformations can share the [4Fe-4S]²⁺ cluster via the CXXC motif of C-domain of NFU1 and CX₆₃CXC motif of ISCA1 (Figures 5B and 6). Specifically, spectroscopic data revealed that both cysteines of the conserved CXXC motif of NFU1 and Cys57 of ISCA1 participate to [4Fe-4S]²⁺ cluster binding, resulting NFU1 cysteines essential to bind the cluster, and that Cys121 or Cys123 of the CX₆₃CXC motif of ISCA1 can compete to complete the coordination sphere of the [4Fe-4S]²⁺ cluster. The structural plasticity of NFU1 might also play a role in the final step of the pathway. Indeed, the [4Fe-4S]²⁺ cluster insertion into the mitochondrial proteins requiring the cluster for their function, such as LIAS³⁰ (Figure 6), can occur via a switch from a compact to an extended NFU1 conformation.

The model shown in Figure 6 also supports that the N-domain of NFU1 may act as modulator of [4Fe-4S]²⁺ cluster transfer: only in the extended conformation, the C-domain can make available the [4Fe-4S]²⁺ cluster for its transfer, while, in the compact conformation, the N-domain closes the gate of access to transfer the [4Fe-4S]²⁺ cluster and thus it protects the cluster from its transfer. This protecting role of the N-domain towards cluster transfer is in agreement with the finding

that the N-domain was previously shown to be essential to obtain a quantitative [4Fe-4S]²⁺ cluster binding on the C-domain.⁵ Indeed, no more than ~50% of [4Fe-4S]²⁺ cluster was loaded in a construct of NFU1 containing only the C-domain, at variance of full-length NFU1 that was fully metalated by the [4Fe-4S]²⁺ cluster.

In conclusion, our study provides a step forward in understanding the ISCA1, ISCA2 and NFU1 association changes required to drive [4Fe-4S]²⁺ cluster insertion into mitochondrial apo recipient proteins along the mitochondrial NFU1-cluster acceptor pathway. The structural snapshots of ISCA1-ISCA2, ISCA1-ISCA2-NFU1 and ISCA1-NFU1 apo complexes, here reported, allowed us to propose that the domain-domain conformational flexibility of NFU1 is a crucial factor to drive protein partner recognition and [4Fe-4S]²⁺ cluster mobilization from the cluster-assembly site in ISCA1-ISCA2 complex to the cluster-transfer site in ISCA1-NFU1 complex. We showed that the latter complex bridges a [4Fe-4S]²⁺ cluster via the CXXC motif of NFU1, Cys 57 of ISCA1 and Cys121 or Cys123 of ISCA1, which can either complete the cluster coordination. We provide a first rationale at the molecular level for the function of the N-domain of NFU1, whose conformational changes likely play a key role in protecting and modulating the [4Fe-4S]²⁺ cluster transfer. We finally wish to stress a critical issue of the present work: the proposed mechanistic modelling is our best interpretation, based on intrinsically low-resolution data, for a high dynamic system involving NFU1, ISCA1 and ISCA2 proteins and complexes. Mixed populations and transient states are to be expected to be present in the samples of these systems, potentially resulting in a wider

range of relevant species than those presented here. Further studies may further disentangle this additional complexity.

Materials and Methods

Sample preparation

Human ^{15}N -labelled NFU1 (residues 59–254), unlabelled ISCA1 (residues 1–129) and ^{15}N -labelled ISCA2 (residues 44–154) in their apo forms were produced following protocols already available in the literature.^{5,21,28} The apo ISCA1-ISCA2, apo ISCA1-NFU1 and apo ISCA1-ISCA2-NFU1 complexes were obtained following previously reported procedures.^{14,28} In brief, ^{15}N -labelled apo NFU1 or ^{15}N -labelled apo ISCA2 were titrated with unlabelled apo ISCA1 up to reach the complete formation of apo ISCA1-ISCA2 and apo ISCA1-NFU1 complexes. The complex formation was followed by NMR monitoring the chemical shift changes on the ^1H - ^{15}N HSQC maps (collected at 298 K on Bruker AVANCE 950 MHz), upon the additions of unlabelled apo ISCA1, and complete complex formation was obtained when no changes on the chemical shifts were observed on the NMR spectra upon sequential unlabelled apo ISCA1 additions. This occurs at a roughly 1:1 ratio, indicating that, at the protein concentrations used in the NMR titrations (in the range of 400–500 μM), the complex formation is stoichiometrically obtained. The formation of the apo ISCA1-ISCA2-NFU1 ternary complex was obtained by titrating the apo unlabelled ISCA1- ^{15}N -labelled ISCA2 complex with ^{15}N -labelled apo NFU1 and following the chemical shift changes of NFU1 signals specifically monitoring the complete formation of the ternary complex, again reached when a \sim 1:1 ratio was reached. All samples were in 50 mM phosphate buffer at pH 7.0, 150 mM NaCl and 5 mM DTT, for their spectroscopic characterization. The used proteins concentrations, determined by the method of Bradford, resulted sufficiently higher to allow monitoring the complexes in the SEC-SAXS measurements.

Site-directed mutagenesis (QuickChange Site-directed Mutagenesis Kit, Agilent Technologies, Milan, Italy) was applied on pETG20A/wild-type NFU1 and pDEST-HisMBP/wild-type ISCA1 expression vectors, already available in the lab, to produce recombinant Cys210Ala and Cys213Ala NFU1 single mutants, and Cys57Ala, Cys121Ala, Cys123Ala ISCA1 single mutants and Cys121Ala/Cys123Ala double mutant. The mutated proteins were produced following the same protocols used for the wild-type proteins.

Synchrotron Small-Angle X-ray scattering

Synchrotron Small-Angle X-ray Scattering data were collected at the EMBL beamline P12⁴³ of the PETRA III storage ring (Hamburg, Germany). The

data collection parameters are summarised in **Table S1**. The SAXS data were collected with a Pilatus 6 M detector at an X-ray energy of 10 keV and a sample-to-detector distance of 3 m, allowing to cover the momentum transfer $s = \frac{4\pi \sin \theta}{\lambda}$ in the range $0.03 \lesssim s < 7.4 \text{ nm}^{-1}$, where 2θ is the scattering angle and λ the X-ray wavelength.

On-line size-exclusion chromatography was employed, routing the eluate of a GE S75 5/150 increase size-exclusion column directly to the 0.9 mm quartz SAXS capillary, thermostated at 20 °C. The running buffer was 50 mM sodium phosphate, 150 mM NaCl, 5 mM DTT, 3% v/v glycerol pH 7.0 (with the DTT added immediately before the runs). During each run of 15 min at 0.3 mL/min flow rate $900 \times 0.995 \text{ s}$ X-ray exposures were collected. The samples were thawed on ice, centrifuged 30 min at 5 °C and 21900 $\times g$ and stored at 10 °C prior to injection of 30 to 50 μL of the protein solutions for each run.

The SAXS data were automatically reduced with SASFLOW,⁴⁴ subtracted SEC-SAXS curves were obtained selecting the appropriate sample and buffer frames using CHROMIXS,⁴⁵ the overall parameters from the subtracted curves evaluated using PRIMUS⁴⁶ and the ATSAS⁴⁷ suite. $P(r)$ functions were calculated using GNOM.⁴⁸

CRY SOL⁴⁹ was used to compute the scattering from the models and fit the SAXS curves. *Ab initio* modelling was performed with DAMMIF⁵⁰ with at least 10 runs per modelled construct, in order to obtain a further estimate of the molecular mass the resulting models were then compared using DAMAVER⁵¹ to identify those most representative protein shape. The visual comparison of the models provided also hints on the possible localized disorder.

Hybrid modelling was performed using CORAL⁴⁶ by refining the quaternary structure and completing the available high-resolution models of the rigid domains with flexible loops and linkers. Flexibility was addressed in detail for NFU1 employing EOM.^{52,53} Models from repeated CORAL runs were superimposed with SUPALM⁵⁴ and classified with DAMCLUST.⁵⁵ The PyMOL Molecular Graphics System, Version 2.3.2 Schrödinger, LLC, was used to visualize and display the models.

Structural coordinates used in CORAL modelling

The structural model of the rigid core of monomeric apo ISCA1, comprising residues 24–117, was obtained by homology modelling based on the crystal structure of the *E. coli* SufA homologue (apo form, PDB code 2D2A³⁶), which is a confident PDB hit for modelling human ISCA1 structure with 59% of sequence similarity. The C-terminal segment comprising residues 118–129 is flexible from the homology model, and the N-terminal segment of apo ISCA1, which comprises residues 1–23 (plus an N-terminal Gly residue

from cloning), is likewise disordered and flexible from the model. A further structural model of monomeric apo ISCA1 was generated by homology modelling based on the crystal structure of the monomer of a bacterial Isca that binds a [2Fe-2S] cluster (holo form, PDB code 1X0G⁵⁶), which orders the C-terminal region where two conserved Cys ligands are located.

The model of apo NFU1 included the structures of the two globular domains of NFU1 (PDB codes 2LTM and 2M5O, respectively²⁹) connected by a linker of 12 dummy residues exposed to the solvent. The four N-terminal dummy residues for the tag present at the N-terminal domain (GlySerPheThr-tag) and 12 C-terminal dummy residues in the C-terminal domain were added as well, and they are disordered and flexible.⁵

To generate a reliable structural model of the apo ISCA1-ISCA2 core, we considered, as previously reported by a NMR study,¹⁴ the residues of apo ISCA2 showing significant backbone chemical shift changes upon apo ISCA1 additions to be involved in the complex interface. The solutions were thus constrained by imposing contacts between the subunits of the heterodimer. Interestingly, these residues are also involved at the interface in the homodimeric structural model of human apo ISCA2 (based on the *E. coli* SufA dimerization mode (apo form, PDB code 2D2A)), which was also shown to fit well to homodimeric ISCA2 solution SAXS data in a previous work.²² On these basis, we can conclude that ISCA2 shares the same subunit-subunit interface in both apo homodimeric ISCA2 and apo heterodimeric ISCA1-ISCA2 complexes, and thus a structural model of the apo ISCA1-ISCA2 core was modelled utilizing apo SufA dimerization mode. In this core, the C-termini of both ISCA1 and ISCA2 are in the same conformation as in the monomeric bacterial Isca template bound to a [2Fe-2S] cluster in order to mimic the cluster bound conformation of the C-terminal segments. The rigid core was complemented using CORAL with the same 23-residue long N-terminal tail of ISCA1 as previously done for the monomer, and five residues for the N-terminal tag of ISCA2 (GlySerPheThrMet-tag). A further structural model of apo ISCA1-ISCA2 core was similarly obtained from the *E. coli* Isca homodimeric structure template (PDB code 1S98, chains 1 and 6⁵⁷) which has a dimeric interface different from that of *E. coli* SufA.

For the hybrid modelling of the apo ISCA1-NFU1 and apo ISCA1-ISCA2-NFU1 complexes, the termini and linkers were added as in the individual components for both complexes. For ISCA1, in both apo ISCA1-NFU1 and apo ISCA1-ISCA2-NFU1 complexes, the model with the folded C-terminus was used (as in apo ISCA1-ISCA2). For the apo ISCA1-NFU1 complex, an alternative model, the same used for modelling the ISCA1 monomer, with the last 12 C-terminal residues of ISCA1 added as dummy residues chain was also

tested since ISCA1 is in this case not bound to ISCA2, and found indeed to yield better fits (shown in this work). The interface found previously between ISCA1 and ISCA2 in the ISCA1-ISCA2 heterodimer was also used to fix the relative orientation of the rigid portion of these subunits within the ternary complex by imposing the same constraints. For both complexes, according to previous NMR data,²⁸ we considered that the NFU1 residues involved at the interface with ISCA1 were those at its C-terminal domain, which indeed showed significant NMR shifts upon titration of apo ¹⁵N-NFU1 with both apo ISCA1 and apo ISCA1-ISCA2 complex, and the contacts set accordingly.

Production, biochemical analysis and spectroscopic characterization of [4Fe-4S]²⁺ cluster-bound ISCA1-NFU1 Cys-mutated complexes

Seven ISCA1-NFU1 complexes were produced mixing a wild-type protein with a Cys to Ala mutant or the wild-type of the protein partner. Specifically, a mixture of apo NFU1 (wild-type, Cys210Ala or Cys213Ala) and ISCA1 (wild-type, Cys57Ala, Cys121Ala, Cys123Ala or Cys121Ala/Cys123Ala mutants) was obtained by stepwise titrating apo ¹⁵N NFU1 with anaerobically purified ISCA1 and monitoring changes in the ¹H-¹⁵N HSQC NMR maps at 900 MHz. Chemical shift changes occur in a slow/intermediate exchange regime on the NMR time scale, which were completed once the ~1:1 protein ratio was reached, as previously observed in the case of the complete formation of the wild-type ISCA1-NFU1 hetero-complex.²⁸ Each complex was then chemically reconstituted in order to obtain the [4Fe-4S]²⁺ cluster-bound hetero-complex. Chemical reconstitution was anaerobically performed in 50 mM Tris-HCl buffer at pH 8.0, 100 mM NaCl and 5 mM DTT adding from six to eight equivalents of FeCl₃ and Na₂S to a protein solution of ~50–100 μM at room temperature. Anaerobic conditions were obtained performing the chemical reconstitution in glove box (MBraun Labstar 130) with less than 2 ppm of oxygen and by using all buffers degassed. The excess of FeCl₃ and Na₂S as well as Fe-S aggregates/precipitates were removed by PD-10 desalting column and the protein complex was recovered in degassed 50 mM phosphate buffer at pH 7.0, 150 mM NaCl and 5 mM DTT for the following spectroscopic characterization. The concentrations of the complexes were determined by the Bradford assay using BSA as the calibration standard. Iron and acid-labile sulfur concentrations were determined using the colorimetric published methods.^{58,59} The chemically reconstituted complex was analysed by UV-visible spectroscopy to check Fe-S cluster binding. Paramagnetic 1D ¹H NMR experiments were performed at 400 MHz with a ¹H optimized 5 mm probe on the complexes that

resulted to have intense UV–visible bands typically characterizing Fe-S cluster binding. These spectra were acquired at 283–308 K by means of the super-WEFT sequence with a recycle time of 65 ms.⁶⁰ The 50 mM phosphate buffer at pH 7.0, 150 mM NaCl, 5 mM DTT, and 10% (v/v) D₂O was degassed.

Accession Numbers

The SAXS data and models are available on <https://www.sasbdb.org> with accession codes: **SASDP98**, **SASDPA8**, **SASDPB8**, **SASDPC8**, **SASDPD8** (see <https://www.sasbdb.org/project/1852/>).

CRedit authorship contribution statement

Stefano Da Vela: Investigation, Methodology, Validation, Visualization. **Giovanni Saudino:** Investigation, Validation. **Francesca Lucarelli:** Investigation. **Lucia Banci:** Project administration, Funding acquisition, Writing – review & editing. **Dmitri I. Svergun:** Funding acquisition, Writing – review & editing. **Simone Ciofi-Baffoni:** Conceptualization, Supervision, Writing – original draft, Writing – review & editing.

DECLARATION OF COMPETING INTEREST

The authors declare that they have no known competing financial interests or personal relationships that could have appeared to influence the work reported in this paper.

Acknowledgements

S.D.V. and D.S. acknowledge Mark A. White (UMTB, Galveston, TX, US) for the idea of showing the EOM results as two-dimensional distributions. The authors acknowledge funding from iNEXT-Discovery, project number 871037, funded by the Horizon 2020 program of the European Commission. L.B. acknowledges the support by the Italian Ministry for University and Research (FOE funding) to the CERMI/CIRMMP Italian Centre of Instruct-ERIC, a ESFRI Landmark.

Appendix A. Supplementary Data

Supplementary data to this article can be found online at <https://doi.org/10.1016/j.jmb.2023.168154>.

Received 1 March 2023;

Accepted 15 May 2023;

Available online 19 May 2023

Keywords:

iron-sulfur protein;

ISCA1;
ISCA2;
SAXS;
protein–protein interaction

† Contributed equally.

‡ Present addresses: University of Applied Science Bremerhaven, An der Karlstadt 8, 27568 Bremerhaven, Germany (Stefano Da Vela); BIOSAXS GmbH, c/o DESY, Notkestrasse 85, 22607 Hamburg, Germany (Dmitri I. Svergun).

Abbreviations:

Fe-S, Iron-sulfur; LIAS, lipoic acid synthase; HSQC, heteronuclear single quantum coherence; SEC-SAXS, small-angle X-ray scattering coupled with on-line size-exclusion chromatography; DTT, 1,4-dithiothreitol; Tris-HCl, Tris(hydroxymethyl) aminomethane hydrochloride; NSD, Normalized spatial discrepancy; R_g, radius of gyration; SEC, size-exclusion chromatography; CORAL, complexes with random loops; P(r), pair distance distribution; EOM, ensemble optimization method

References

- Ciofi-Baffoni, S., Nasta, V., Banci, L., (2018). Protein networks in the maturation of human iron-sulfur proteins. *Metalomics* **10**, 49–72.
- Lill, R., Freibert, S.A., (2020). Mechanisms of Mitochondrial Iron-Sulfur Protein Biogenesis. *Annu. Rev. Biochem* **89**, 471–499.
- Maio, N., Rouault, T.A., (2020). Outlining the Complex Pathway of Mammalian Fe-S Cluster Biogenesis. *Trends Biochem. Sci* **45**, 411–426.
- Cai, K., Frederick, R.O., Markley, J.L., (2020). ISCU interacts with NFU1, and ISCU[4Fe-4S] transfers its Fe-S cluster to NFU1 leading to the production of holo-NFU1. *J. Struct. Biol.* **210**, 107491
- Nasta, V., Suraci, D., Gourdupis, S., Ciofi-Baffoni, S., Banci, L., (2020). A pathway for assembling [4Fe-4S]²⁺ clusters in mitochondrial iron-sulfur protein biogenesis. *FEBS J.* **287**, 2312–2327.
- Beilschmidt, L.K., Ollagnier de Choudens, S., Fournier, M., Sanakis, I., Hograindeur, M.A., Clemancey, M., et al., (2017). ISCA1 is essential for mitochondrial Fe4S4 biogenesis in vivo. *Nature Commun.* **8**, 15124.
- Sheftel, A.D., Wilbrecht, C., Stehling, O., Niggemeyer, B., Elsasser, H.P., Muhlenhoff, U., et al., (2012). The human mitochondrial ISCA1, ISCA2, and IBA57 proteins are required for [4Fe-4S] protein maturation. *Mol. Biol. Cell* **23**, 1157–1166.
- Melber, A., Na, U., Vashisht, A., Weiler, B.D., Lill, R., Wohlschlegel, J.A., et al., (2016). Role of Nfu1 and Bol3 in iron-sulfur cluster transfer to mitochondrial clients. *Elife* **5**, e15991.
- Jain, A., Singh, A., Maio, N., Rouault, T.A., (2020). Assembly of the [4Fe-4S] cluster of NFU1 requires the coordinated donation of two [2Fe-2S] clusters from the scaffold proteins, ISCU2 and ISCA1. *Hum. Mol. Genet.* **29**, 3165–3182.
- Gervason, S., Larkem, D., Mansour, A.B., Botzanowski, T., Müller, C.S., Pecqueur, L., et al., (2019). Physiologically relevant reconstitution of iron-sulfur cluster biosynthesis

- uncovers persulfide-processing functions of ferredoxin-2 and frataxin. *Nature Commun.* **10**, 3566.
11. Boniecki, M.T., Freibert, S.A., Muhlenhoff, U., Lill, R., Cygler, M., (2017). Structure and functional dynamics of the mitochondrial Fe/S cluster synthesis complex. *Nature Commun.* **8**, 1287.
 12. Freibert, S.A., Boniecki, M.T., Stümpfig, C., Schulz, V., Krapoth, N., Winge, D.R., et al., (2021). N-terminal tyrosine of ISCU2 triggers [2Fe-2S] cluster synthesis by ISCU2 dimerization. *Nature Commun.* **12**, 6902.
 13. Patra, S., Barondeau, D.P., (2019). Mechanism of activation of the human cysteine desulfurase complex by frataxin. *PNAS* **116**, 19421–19430.
 14. Brancaccio, D., Gallo, A., Mikolajczyk, M., Zovo, K., Palumaa, P., Novellino, E., et al., (2014). Formation of [4Fe-4S] clusters in the mitochondrial iron-sulfur cluster assembly machinery. *J. Am. Chem. Soc.* **136**, 16240–16250.
 15. Weiler, B.D., Brück, M.C., Kothe, I., Bill, E., Lill, R., Mühlhoff, U., (2020). Mitochondrial [4Fe-4S] protein assembly involves reductive [2Fe-2S] cluster fusion on ISCA1-ISCA2 by electron flow from ferredoxin FDX2. *PNAS* **117**, 20555–20565.
 16. Navarro-Sastre, A., Tort, F., Stehling, O., Uzarska, M.A., Arranz, J.A., Del, T.M., et al., (2011). A fatal mitochondrial disease is associated with defective NFU1 function in the maturation of a subset of mitochondrial Fe-S proteins. *Am. J. Hum. Genet.* **89**, 656–667.
 17. Cameron, J.M., Janer, A., Levandovskiy, V., MacKay, N., Rouault, T.A., Tong, W.H., et al., (2011). Mutations in iron-sulfur cluster scaffold genes NFU1 and BOLA3 cause a fatal deficiency of multiple respiratory chain and 2-oxoacid dehydrogenase enzymes. *Am. J. Hum. Genet.* **89**, 486–495.
 18. Camponeschi, F., Ciofi-Baffoni, S., Calderone, V., Banci, L., (2022). Molecular Basis of Rare Diseases Associated to the Maturation of Mitochondrial [4Fe-4S]-Containing Proteins. *Biomolecules* **12**, 1009.
 19. Saudino, G., Suraci, D., Nasta, V., Ciofi-Baffoni, S., Banci, L., (2021). Molecular Basis of Multiple Mitochondrial Dysfunctions Syndrome 2 Caused by CYS59TYR BOLA3 Mutation. *Int. J. Mol. Sci.* **22**, 4848.
 20. Brancaccio, D., Gallo, A., Piccioli, M., Novellino, E., Ciofi-Baffoni, S., Banci, L., (2017). [4Fe-4S] Cluster Assembly in Mitochondria and Its Impairment by Copper. *J. Am. Chem. Soc.* **139**, 719–730.
 21. Banci, L., Brancaccio, D., Ciofi-Baffoni, S., Del Conte, R., Gadepalli, R., Mikolajczyk, M., et al., (2014). [2Fe-2S] cluster transfer in iron-sulfur protein biogenesis. *PNAS* **111**, 6203–6208.
 22. Nasta, V., Da Vela, S., Gourdupis, S., Ciofi-Baffoni, S., Svergun, D.I., Banci, L., (2019). Structural properties of [2Fe-2S] ISCA2-IBA57: a complex of the mitochondrial iron-sulfur cluster assembly machinery. *Sci. Rep.* **9**, 18986.
 23. Gourdupis, S., Nasta, V., Calderone, V., Ciofi-Baffoni, S., Banci, L., (2018). IBA57 Recruits ISCA2 to Form a [2Fe-2S] Cluster-Mediated Complex. *J. Am. Chem. Soc.* **140**, 14401–14412.
 24. Nasta, V., Giachetti, A., Ciofi-Baffoni, S., Banci, L., (2017). Structural insights into the molecular function of human (2Fe-2S) BOLA1-GRX5 and (2Fe-2S) BOLA3-GRX5 complexes. *BBA* **1861**, 2119–2131.
 25. Melber, A., Winge, D.R., (2018). Steps Toward Understanding Mitochondrial Fe/S Cluster Biogenesis. *Methods Enzymol.* **599**, 265–292.
 26. Uzarska, M.A., Nasta, V., Weiler, B.D., Spantgar, F., Ciofi-Baffoni, S., Saviello, M., et al., (2016). Mitochondrial Bol1 and Bol3 function as assembly factors for specific iron-sulfur proteins. *Elife* **5**, e16673.
 27. Tong, W.H., Jameson, G.N., Huynh, B.H., Rouault, T.A., (2003). Subcellular compartmentalization of human Nfu, an iron-sulfur cluster scaffold protein, and its ability to assemble a [4Fe-4S] cluster. *PNAS* **100**, 9762–9767.
 28. Suraci, D., Saudino, G., Nasta, V., Ciofi-Baffoni, S., Banci, L., (2021). ISCA1 Orchestrates ISCA2 and NFU1 in the Maturation of Human Mitochondrial [4Fe-4S] Proteins. *J. Mol. Biol.* **433**, 166924.
 29. Cai, K., Liu, G., Frederick, R.O., Xiao, R., Montelione, G.T., Markley, J.L., (2016). Structural/Functional Properties of Human NFU1, an Intermediate [4Fe-4S] Carrier in Human Mitochondrial Iron-Sulfur Cluster Biogenesis. *Structure* **24**, 2080–2091.
 30. Saudino, G., Ciofi-Baffoni, S., Banci, L., (2022). Protein-Interaction Affinity Gradient Drives [4Fe-4S] Cluster Insertion in Human Lipoyl Synthase. *J. Am. Chem. Soc.* **144**, 5713–5717.
 31. Graewert, M.A., Da Vela, S., Grawert, T.W., Molodenskiy, D.S., Blanchet, C.E., Svergun, D.I., et al., (2020). Adding Size Exclusion Chromatography (SEC) and Light Scattering (LS) Devices to Obtain High-Quality Small Angle X-Ray Scattering (SAXS) Data. *Crystals* **10**
 32. Kozin, M.B., Svergun, D.I., (2001). Automated matching of high- and low-resolution structural models. *Journal of applied crystallography. J. Appl. Cryst.* **34**, 33–41.
 33. Erdős, G., Pajkos, M., Dosztányi, Z., (2021). IUPred3: prediction of protein disorder enhanced with unambiguous experimental annotation and visualization of evolutionary conservation. *Nucleic Acids Res.* **49**, W297–W303.
 34. Torraco, A., Stehling, O., Stümpfig, C., Rösser, R., De Rasmio, D., Fiermonte, G., et al., (2018). ISCA1 mutation in a patient with infantile-onset leukodystrophy causes defects in mitochondrial [4Fe-4S] proteins. *Hum. Mol. Genet.* **27**, 2739–2754.
 35. Jumper, J., Evans, R., Pritzel, A., Green, T., Figurnov, M., Ronneberger, O., et al., (2021). Highly accurate protein structure prediction with AlphaFold. *Nature* **596**, 583–589.
 36. Wada, K., Hasegawa, Y., Gong, Z., Minami, Y., Fukuyama, K., Takahashi, Y., (2005). Crystal structure of Escherichia coli SufA involved in biosynthesis of iron-sulfur clusters implications for a functional dimer. *FEBS Letter* **579**, 6543–6548.
 37. Evans, R., O'Neill, M., Pritzel, A., Antropova, N., Senior, A., Green, T., et al., (2021). Protein complex prediction with AlphaFold-Multimer. *bioRxiv the preprint server for biology*. 2021.2010.2004.463034.
 38. Agar, J.N., Krebs, C., Frazzon, J., Huynh, B.H., Dean, D. R., Johnson, M.K., (2000). IscU as a scaffold for iron-sulfur cluster biosynthesis: sequential assembly of [2Fe-2S] and [4Fe-4S] clusters in IscU. *Biochemistry* **39**, 7856–7862.
 39. Banci, L., Camponeschi, F., Ciofi-Baffoni, S., Piccioli, M., (2018). The NMR contribution to protein-protein networking in Fe-S protein maturation. *J. Biol. Inorg. Chem.* **23**, 687.
 40. Camponeschi, F., Muzzioli, R., Ciofi-Baffoni, S., Piccioli, M., Banci, L., (2019). Paramagnetic (1)H NMR Spectroscopy to Investigate the Catalytic Mechanism of

- Radical S-Adenosylmethionine Enzymes. *J. Mol. Biol.* **431**, 4514–4522.
41. Bertini, I., Capozzi, F., Luchinat, C., Piccioli, M., (1993). ¹H NMR investigation of oxidized and reduced HiPIP from *R. globiformis*. *Eur. J. Biochem.* **212**, 69–78.
 42. Bentrop, D., Bertini, I., Capozzi, F., Dikiy, A., Eltis, L.D., Luchinat, C., (1996). Three dimensional structure of the reduced C77S mutant of the *Chromatium vinosum* high potential iron-sulfur protein through NMR. Comparison with the solution structure of the wild-type protein. *Biochemistry* **35**, 5928–5936.
 43. Blanchet, C.E., Spilotros, A., Schwemmer, F., Graewert, M.A., Kikhney, A., Jeffries, C.M., et al., (2015). Versatile sample environments and automation for biological solution X-ray scattering experiments at the P12 beamline (PETRA III, DESY). *J. Appl. Cryst.* **48**, 431–443.
 44. Franke, D., Kikhney, A.G., Svergun, D.I., (2012). Automated acquisition and analysis of small angle X-ray scattering data. *Nucl Instrum Meth A* **689**, 52–59.
 45. Panjkovich, A., Svergun, D.I., (2018). CHROMIXS: automatic and interactive analysis of chromatography-coupled small-angle X-ray scattering data. *Bioinformatics* **34**, 1944–1946.
 46. Petoukhov, M.V., Franke, D., Shkumatov, A.V., Tria, G., Kikhney, A.G., Gajda, M., et al., (2012). New developments in the ATSAS program package for small-angle scattering data analysis. *J. Appl. Cryst.* **45**, 342–350.
 47. Manalastas-Cantos, K., Konarev, P.V., Hajizadeh, N.R., Kikhney, A.G., Petoukhov, M.V., Molodenskiy, D.S., et al., (2021). ATSAS 3.0: expanded functionality and new tools for small-angle scattering data analysis. *J. Appl. Cryst.* **54**, 343–355.
 48. Svergun, D.I., (1992). Determination of the regularization parameter in indirect-transform methods using perceptual criteria. *J. Appl. Cryst.* **25**, 495–503.
 49. Svergun, D.I., Barberato, C., Koch, M.H.J., (1995). CRY SOL - a program to evaluate X-ray solution scattering of biological macromolecules from atomic coordinates. *J. Appl. Cryst.* **28**, 768–773.
 50. Franke, D., Svergun, D.I., (2009). DAMMIF, a program for rapid ab-initio shape determination in small-angle scattering. *J. Appl. Cryst.* **42**, 342–346.
 51. Volkov, V.V., Svergun, D.I., (2003). Uniqueness of ab initio shape determination in small-angle scattering. *J. Appl. Cryst.* **36**, 860–864.
 52. Tria, G., Mertens, H.D., Kachala, M., Svergun, D.I., (2015). Advanced ensemble modelling of flexible macromolecules using X-ray solution scattering. *IUCrJ* **2**, 207–217.
 53. Sagar, A., Jeffries, C.M., Petoukhov, M.V., Svergun, D.I., Bernadó, P., (2021). Comment on the Optimal Parameters to Derive Intrinsically Disordered Protein Conformational Ensembles from Small-Angle X-ray Scattering Data Using the Ensemble Optimization Method. *J. Chem. Theory Comput.* **17**, 2014–2021.
 54. Konarev, P.V., Petoukhov, M.V., Svergun, D.I., (2016). Rapid automated superposition of shapes and macromolecular models using spherical harmonics. *J. Appl. Cryst.* **49**, 953–960.
 55. Petoukhov, M.V., Franke, D., Shkumatov, A.V., Tria, G., Kikhney, A.G., Gajda, M., et al., (2012). New developments in the ATSAS program package for small-angle scattering data analysis. *J. Appl. Cryst.* **45**, 342–350.
 56. Morimoto, K., Yamashita, E., Kondou, Y., Lee, S.J., Arisaka, F., Tsukihara, T., et al., (2006). The asymmetric IscA homodimer with an exposed [2Fe-2S] cluster suggests the structural basis of the Fe-S cluster biosynthetic scaffold. *J. Mol. Biol.* **360**, 117–132.
 57. Cupp-Vickery, J.R., Silberg, J.J., Ta, D.T., Vickery, L.E., (2004). Crystal structure of IscA, an iron-sulfur cluster assembly protein from *Escherichia coli*. *J. Mol. Biol.* **338**, 127–137.
 58. Banci, L., Bertini, I., Ciofi-Baffoni, S., Boscaro, F., Chatzi, A., Mikołajczyk, M., et al., (2011). Anamorsin is a 2Fe2S cluster-containing substrate of the Mia40-dependent mitochondrial protein trapping machinery. *Chem. Biol.* **18**, 794–804.
 59. Roland, M., Przybyla-Toscano, J., Vignols, F., Berger, N., Azam, T., Christ, L., et al., (2020). The plastidial *Arabidopsis thaliana* NFU1 protein binds and delivers [4Fe-4S] clusters to specific client proteins. *J. Biol. Chem.* **295**, 1727–1742.
 60. Inubushi, T., Becker, E.D., (1983). Efficient detection of paramagnetically shifted NMR resonances by optimizing the WEFT pulse sequence. *J. Magn. Reson.* **51**, 128–133.
 61. Franke, D., Petoukhov, M.V., Konarev, P.V., Panjkovich, A., Tuukkanen, A., Mertens, H.D.T., et al., (2017). ATSAS 2.8: a comprehensive data analysis suite for small-angle scattering from macromolecular solutions. *J. Appl. Cryst.* **50**, 1212–1225.